

Development and Validation of a Physically Based ELA Model and Its  
Application to the Younger Dryas Event in the  
Graubünden Alps, Switzerland

Durban Gregg Keeler

A thesis submitted to the faculty of  
Brigham Young University  
in partial fulfillment of the requirements for the degree of

Master of Science

Summer B. Rupper, Chair  
Barry Bickmore  
Jani Radebaugh

Department of Geological Sciences

Brigham Young University

December 2015

Copyright © 2015 Durban Gregg Keeler

All Rights Reserved

## ABSTRACT

### Development and Validation of a Physically Based ELA Model and Its Application to the Younger Dryas Event in the Graubünden Alps, Switzerland

Durban Gregg Keeler  
Department of Geological Sciences, BYU  
Master of Science

The rapid rate of global warming currently underway highlights the need for a deeper understanding of abrupt climate change. The Younger Dryas is a Late-Glacial climate event of widespread and unusually rapid change whose study can help us address this need for increased understanding. Reconstructions from the glacial record offer important contributions to our understanding of the Younger Dryas due to (among other things) the direct physical response of glaciers to even minor perturbations in climate. Because the glacier equilibrium line altitude (ELA) provides a more explicit comparison of climate than properties such as glacier length or area, ELA methods lend themselves well to paleoclimate applications and allow for more direct comparisons in space and time. Here we present a physically based ELA model for alpine paleoglacier climate reconstructions that accounts for differences in glacier width, glacier shape, bed topography and ice thickness, and includes error estimates using Monte Carlo simulations. We validate the ELA model with published mass balance measurements from 4 modern glaciers in the Swiss Alps. We then use the ELA model, combined with a temperature index model, to estimate the changes in temperature and precipitation between the Younger Dryas (constrained by  $^{10}\text{Be}$  surface exposure ages) and the present day for three glacier systems in the Graubünden Alps. Our results indicate an ELA depression in this area of  $320\text{ m} \pm 51\text{ m}$  during the Younger Dryas relative to today. This ELA depression represents annual mean temperatures  $2.29\text{ }^{\circ}\text{C} \pm 1.32\text{ }^{\circ}\text{C}$  cooler relative to today in the region, which corresponds to a decrease in mean summer temperatures of  $1.47\text{ }^{\circ}\text{C} \pm 0.73\text{ }^{\circ}\text{C}$ . Our results indicate relatively small changes in summer temperature dominate over other climate changes for the Younger Dryas paleoglaciers in the Alps. This ELA-based paleoclimate reconstruction offers a simple, fast, and cost-effective alternative to many other paleoclimate reconstruction methods. Continued application of the ELA model to more regions will lead to an improved understanding of the Younger Dryas in the Alps, and by extension, of rapid climate events generally.

Keywords: Younger Dryas, ELA model, paleoclimate, Swiss Alps, cosmogenic radionuclide ages

## TABLE OF CONTENTS

LIST OF TABLES .....	iv
LIST OF FIGURES .....	v
1 INTRODUCTION .....	1
2 BACKGROUND .....	3
2.1 The Younger Dryas.....	3
2.2 Glacier chronologies .....	5
2.3 Equilibrium Line Model .....	7
3 METHODOLOGY .....	11
3.1 ELA model .....	13
3.1.1 Glacier bed modeling.....	13
3.1.2 Glacier width modeling.....	14
3.1.3 Ice thickness modeling.....	16
3.2 Monte Carlo Simulations .....	17
3.3 ELA Estimates from Snowlines .....	17
3.4 Temperature and precipitation reconstructions .....	21
4 RESULTS .....	25
4.1 ELA model validation .....	25
4.1.1 Data sources .....	26
4.1.2 Model outputs .....	29
4.1.3 Snowline ELA proxy results.....	32
4.1.4 ELA comparisons.....	34
4.2 Paleoglacier ELA reconstructions .....	37
4.2.1 Age constraints.....	39
4.2.2 ELA Model outputs.....	40
4.2.3 ELA and $\Delta$ ELA comparisons .....	44
4.2.4 Temperature and precipitation reconstructions.....	47
5 DISCUSSION .....	49
6 CONCLUSIONS.....	52
7 REFERENCES .....	54

## LIST OF TABLES

Table 1. Summary of proxy ELA estimates from snowline analysis .....	34
Table 2. ELA validation tests with associated error .....	37
Table 3. Summary of ages and ELAs for Lagrev, Alp Flix 1, and Alp Flix 2 glaciers .....	47
Table 4. Summary of Younger Dryas temperature reconstructions (various methodologies) ....	51

## LIST OF FIGURES

Figure 1. Plots comparing model performance for glacier beds of varying complexity. ....	14
Figure 2. Comparison of model width initial guess vs. optimal fit.....	15
Figure 3. Example of the misclassification of cloud cover as ice.....	19
Figure 4. Example of misclassification of water as ice. ....	20
Figure 5. Probability density function of a snowline distribution that includes a misclassified water body (Figure 4).....	20
Figure 6. Comparison of modeled temperature throughout the year (red) and actual observed average monthly temperature in south central Switzerland from 1981-2010 (blue). ....	24
Figure 7. Index map showing the locations of validation and paleoclimate reconstruction glaciers. ....	26
Figure 8. Satellite and aerial photographs of the four test glaciers in the Alps: A) Rhone Glacier, B) Findel Glacier, C) Gries Glacier, and D) Silvretta Glacier.....	28
Figure 9. Bed elevation reconstructions for the four validation sites. ....	29
Figure 10. Glacier width modeling for the four validation sites.....	30
Figure 11. Modeled glacier ice surfaces for the four validation glaciers.....	32
Figure 12. Map depicting areas over which summer snowline was calculated for the validation glaciers. ....	34
Figure 13. Probability density functions (PDF) for ELA results from the ELA model (solid lines), mass balance measurements (dashed lines), and snowline estimates (hashed lines).....	36
Figure 14. Aerial photographs for the three glacial valleys used in this study.....	38
Figure 15. Probability density functions for 10Be ages of moraines in Alp Flix 1, Alp Flix 2, and Lagrev. ....	39
Figure 16. Model outputs for Younger Dryas glacier Alp Flix 1. ....	41
Figure 17. Model outputs for Younger Dryas glacier Alp Flix 2. ....	42
Figure 18. Model outputs for the Younger Dryas glacier in Julier Pass (Lagrev Glacier). ....	43
Figure 19. Model outputs for the modern glacier in Julier Pass .....	44
Figure 20. Probability density functions for Younger Dryas absolute ELAs (A) and $\Delta$ ELAs between the Younger Dryas and present day (B) .....	46
Figure 21. Modeled range in changes in temperature and precipitation between the Younger Dryas and present day for the Lagrev Glacier. ....	49

## 1 INTRODUCTION

Climate is a dominating force in our lives, with economic, political, and societal consequences to both individuals and nations. Indeed, the rise and fall of whole societies and civilizations resulted at least in part from changes to climate (Mayewski et. al., 2004). Climate systems, however, even during relatively stable times, represent complex interactions not fully understood at some fundamental levels. Particularly in light of rapid recent global warming, understanding natural climate variability and its driving mechanisms is an increasingly important research target. Although the drivers involved in modern climate change are not necessarily equivalent to the forcings of prior changes, a better understanding of climate in the past, particularly events of abrupt climate disruptions, facilitates our understanding of and predictive power over *future* changes. A study of such climate fluctuations helps us better understand the timing, extent, and mechanisms of climate change in the recent geologic past, improving our understanding of natural climate variability and providing historical context for recent, anthropogenic changes.

Glaciers are important tools in such paleoclimatic reconstructions. Although these records are only one of many used for climate reconstructions, the unique combination of large spatial footprint, direct response to climate, and near-global extent make them indispensable tools (Rupper et al 2009; Nussbaumer et al 2011). In regions of high glacier prevalence and density, glacial histories provide excellent indications of past climate and insight into the spatial variability of changes (Zemp et. al, 2007; Heiri et. al., 2014). In addition, a sufficiently detailed regional glacier record allows for better comparisons of climate sensitivity to regional and global forcings.

Although previous changes to glaciers are often readily apparent qualitatively (Heiri et al., 2014), a direct, quantitative comparison of climate between different glacier valleys or even different events in the same valley proves more difficult. Quantifying changes in climate from glaciers has two primary challenges. First, defining glacier “change” itself can be somewhat ambiguous. Geomorphic variations can be quantified as a change in mass, length or area, to name a few. Second, the translation of these glacier variations to changes in climate is equally difficult. Glaciers respond to changes in mass balance, but the response of glacier area and length depends not only on the magnitude of the mass balance changes, but also on factors such as the topographic and hypsometric setting (Benn and Lehmkuhl, 2000). In other words, two glaciers that experience the same mass balance changes will not necessarily exhibit the same area or length change. Similarly, the mass balance is a complex function of the climate. Two glaciers within two different climatic and topographic settings may have significantly different responses even when forced with the same magnitude of climate change. Thus, simple comparisons of changes in overall glacier length or area are an inaccurate proxy for the true change in climate conditions. These complications have led to significant variability in the reported connections between glaciers and climate, complicating any direct comparisons from one region or time to the next.

Here we present a new, robust model to reconstruct changes in climate based on changes in glacier geometry and hypsometry. The methodology presented here retains the simplicity of many other paleoclimate reconstructions, but further incorporates physically based assumptions that relate this estimate more directly and generally to glacier mass balance than statistical approaches. We validate this model against present-day glacier systems in the Alps using published mass balance measurements. We then apply this model to three Swiss Younger Dryas

moraine sequences (constrained using  $^{10}\text{Be}$  surface exposure ages), and estimate the underlying *changes in temperature and precipitation* using an ablation and temperature index model.

## 2 BACKGROUND

### 2.1 The Younger Dryas

Particularly in light of present concerns with anthropogenic warming, understanding the fundamental mechanisms in abrupt changes in our climate continues to grow in importance. The Younger Dryas cold interval, named after the Arctic-alpine flower (*Dryas octopetala*) used to first identify it, is one of the most prevalent and extensively studied examples of abrupt climate change (Overpeck and Cole, 2006 and references therein; Carlson, 2013). The Younger Dryas occurred at the final stage of the Pleistocene, representing a rapid reversal of the warming since the Last Glacial Maximum to return to near full-glacial conditions (Overpeck and Cole, 2006). Many records show a rapid onset of the Younger Dryas on the order of decades or less (Alley and Agustsdottir, 2005), making it one of the most spectacular examples of abrupt climate disruption in recent time. Radiocarbon ages place the onset of the Younger Dryas in Europe at 12.9 ka and the termination to 11.7 ka (Carlson, 2013), although the exact timing varies regionally. The termination of the Younger Dryas cold interval in Greenland ice cores also defines the start of the Holocene Epoch (Walker et. al., 2008).

The Younger Dryas has received intense study in recent years due to the rapidity, magnitude, and extent of the event and has served as a primary target for the investigations of tipping points in the climate system (Broecker, 1997; Alley et. al., 2003). Despite such concerted focus, many questions remain as to the nature, cause, and internal mechanisms of this abrupt change. The predominant theory explains these changes as driven by weakening of the Atlantic

meridional overturning circulation (AMOC), likely resulting from increased influx of fresh water to the Atlantic Ocean (Broecker, 1997, Overpeck and Cole, 2006). A comprehensive solution to the precise interactions of factors involved, however, remains elusive, and even the mechanism itself remains debated. The resolution of these issues has important implications for our general understanding of climatic tipping points and abrupt climate change.

In order to address these questions, many researchers investigate the potential patterns in temporal and spatial variability of climate response during the Younger Dryas (e.g. Ivy-Ochs et. al., 2007; Zech et. al., 2007; Doughty et. al., 2013). Such studies hope to shed further light on the underlying mechanisms, with increased data coverage and density leading to the elimination of incorrect hypotheses. The full global extent of the Younger Dryas, however, is still a matter of debate, as is the magnitude and timing of the response in diverse regions. Overpeck and Cole (2006) note the Younger Dryas is relatively well documented in the Northern Hemisphere, with particularly well-defined signals in the North Atlantic and Europe. Even in areas such as, debate continues over the magnitude and variability of the event, and therefore the exact nature and details of the underlying driving factors.

The complex and somewhat convoluted response of the Southern Hemisphere to the Younger Dryas adds additional confusion. Some records demonstrate a cooling period, referred to as the Antarctic Cold Reversal (ACR), prior to the Younger Dryas, with warming and glacier retreat in the Southern Hemisphere during the Younger Dryas (Kaplan et. al., 2010; Doughty et. al., 2013). Whether these relationships are coincidental or causal, and the underlying mechanisms connecting these events, remains an unresolved question. The magnitude of the Younger Dryas response within and between different regions is another area of current debate. Some argue this spatial variability is driven by regional differences in precipitation (Kerschner,

2000), while others present evidence of changes in wintertime temperature as a likely culprit (Denton et. al., 2005). Such investigations are hampered by sparse and, at times, contradictory data. Increased sources of temporally constrained, robust climate reconstructions, particularly data that are directly comparable, would help resolve these issues. By so doing, we increase our understanding of abrupt climate change both in the past and the future.

## *2.2 Glacier chronologies*

The glacier record is an excellent candidate to help address many of these issues. Reliable age constraints for glacial advances, however, have typically limited the role of these records in addressing the Younger Dryas or similar abrupt climate events (Goehring et al, 2012). This partially results from the large spatial and temporal variability inherent in the glacier record (e.g. Kaplan et al, 2010; Ivy-Ochs et al, 2009; Schaefer et al, 2009), but just as important is a previous lack of sufficient dating techniques for glacier advances, with only relatively recent analytical techniques available to address this on a large scale (Gosse and Phillips, 2001). Radiocarbon dating is possible in some circumstances where organic debris is present in the ice, but complete records obtained in such a way are rare (Briner, 2011, Goehring et al, 2012, Heiri et. al., 2014). Other methods, such as sedimentation rates in proglacial lakes, only yield approximate bounds for glaciation rather than specific ages of stabilization (Goehring et al, 2012).

This lack of precision in glacial timing leads to ambiguity over the causes of these climate events (Heiri et. al., 2014). Accurate chronologies are prerequisite to developing relationships between glacial advances and potential drivers. This is particularly true in regards to abrupt climate changes because they necessarily require greater temporal resolution. To help address the need for more accurate glacial chronologies, new analytical techniques for dating

glacial deposits have been put forward. One technique, which recently gained widespread use, is surface exposure dating (SED) based on cosmogenic radionuclides. This technique measures isotopes produced in a sample from exposure to nuclear spallation products resulting from interactions with cosmic radiation. By comparing the amount of nuclides generated in the sample to cosmogenic production rates, an absolute age of exposure can be determined for the sample (Gosse and Phillips, 2001). Furthermore, SED techniques directly determine moraine formation, rather than simply yielding upper or lower age bounds (Gosse et. al., 1995).

Among the various terrestrial cosmogenic nuclides,  $^{10}\text{Be}$  is often used to date moraine deposits [e.g. Briner, 2011; Schaefer et al, 2009; Ivy-Ochs, 2009]. This isotope forms due to the collision of  $^{16}\text{O}$  atoms with spallation products from the Earth's atmosphere (Gosse and Phillips, 2001).  $^{16}\text{O}$  is also the main isotope in common quartz ( $\text{SiO}_2$ ). Since this mineral is abundantly present in rocks around the world, quartz often serves as the primary target for  $^{10}\text{Be}$  moraine age measurements (Briner, 2011). A further advantage of  $^{10}\text{Be}$  dating of quartz results from the cosmogenic mutation of  $^{28}\text{Si}$  to  $^{26}\text{Al}$  (Gosse and Phillips, 2001). This allows for a second internal age constraint from the same sample when deemed necessary. Analytical difficulties in accurately measuring the very low levels of  $^{10}\text{Be}$  in glacial deposits prevented the widespread use of in-situ terrestrial cosmogenic dating in the Late Glacial/Holocene record until  $\sim 20$  years ago (Briner, 2011). The advent of surface exposure dating techniques has led to unprecedented precision in determining the absolute age of past glacial events directly from moraine surfaces. Such age constraints are now applied to an ever-increasing number of areas, allowing regional climate events to be placed in a proper temporal context.

### *2.3 Equilibrium Line Model*

Even with properly constrained ages for glacial advances, some method is necessary to extract useful climate information from the changes in glacier size and extent recorded in the landscape (Rupper et al, 2009). Numerous approaches attempt to address this issue, tailored for a wide variety of circumstances. Some approaches suitable to modern applications are difficult to implement in studies of paleoclimate. Estimating required variables for surface energy models (e.g., humidity, surface albedo, atmospheric emissivity) and similarly complex methodologies, especially for paleoclimate conditions, remains a challenge. Likewise, estimates based on maximum summer snowline altitude can be useful for modern glaciers, but are not applicable to prehistoric climate conditions (Leonard and Fountain, 2003; Cuffey and Paterson, 2010).

The lack of detailed climatic data in the past typically requires paleoclimate studies to focus on computationally simple methods of reconstruction, often based on changes in a glacier's geomorphic extent (Cuffey and Paterson, 2010). Comparisons of changes in glacier length or area can give a rough qualitative sense of the relative magnitude of climate change, but are inadequate for truly quantitative analyses. Such measures are not only affected by changes in glacier mass balance, but also by the internal dynamics and geographic setting of the glacier. A more direct measure of climate than glacier area or length changes often used in paleoclimate studies in particular (Benn and Lehmkuhl, 2000; Kerschner and Ivy-Ochs, 2008) is the concept of the equilibrium line altitude (ELA). The ELA is the boundary between the accumulation and ablation zones on a glacier and represents the elevation at which the annual mass budget of the glacier is in equilibrium. In other words, at the ELA the annual amount of mass added through accumulation exactly equals the annual amount of mass lost through ablation. The ELA, as a direct measure of annual glacier mass balance, facilitates more direct comparisons of climate by

avoiding strong dependencies on glacier dynamics, complications regarding the hypsometric distribution of mass on a glacier, and by integrating the myriad variables that can drive changes in climate into a single metric.

Many of the methods used to estimate the ELA provide only an approximate statistical relationship between changes in glacier extent and the ELA. Such statistical models are useful within many contexts, but have certain inherent limitations. Because they are derived from an aggregate glacier data set, these models are only valid for glaciers within the boundary conditions of the training data, typically with no a priori technique to determine whether such an assumption is valid when applied to other regions or other periods of time (Kerschner, 2005; Osmaston, 2005). Some of the most common ELA methods employed are the accumulation area ratio (AAR), the toe to headwall altitude ratio (THAR), the balance ratio (BR), the maximum elevation of lateral moraines (MELM), and cirque floor altitudes. Each of these methods are useful within certain situations, but each also has inherent shortcomings.

The AAR method assumes some fixed ratio exists between the area of the accumulation zone of a glacier and the area of the ablation zone. This method is widely used because of the few necessary inputs, only requiring estimates of the glacier's outline and ice surface elevation (Benn and Lehmkuhl, 2000). The assumed ratio between the accumulation and ablation areas, however, is simply a statistical relation, requiring tuning to the specific climate regime, topographic setting, and glacier type (e.g. alpine, temperate, piedmont) in question (Braithwaite, 1984; Benn and Lehmkuhl, 2000). Since climate reconstructions are often the goal of such studies, this method involves some risk of circular reasoning, yielding climate reconstructions based in part on assumptions of the climate at the time. AAR values vary globally between 0.22 and 0.72 (with 0.5-0.7 more typical of alpine mid-latitude glaciers), resulting in a large range in

possible ELA estimates depending on the value chosen (Zemp et. al., 2007). Regions are often assigned an average AAR value based on empirical observations of multiple glaciers within a given region. For instance, the Swiss Alps are often assumed to have an AAR of 0.67 (Gross et. al., 1976). Specific glaciers, however, can deviate widely from one another, even within the same region, with no mechanism to account for or estimate these variances (Benn and Lehmkuhl, 2000). Additionally, one cannot determine a priori whether climate conditions influencing the AAR in the present for a given region are the same as they were previously. No guarantee, therefore, exists that an AAR tuned to a modern region is applicable to paleoglaciers.

The other common methods for ELA reconstructions suffer from many similar concerns as the AAR method. The THAR method, for example, also assumes the ELA is some fixed ratio, in this case between the maximum and minimum elevations of a glacier, varying between ~0.3-0.8. The cirque valley floor method diverges from the AAR and THAR approaches. This method assumes the ELA for Pleistocene glaciers is at the level of cirque valley floors. These basins, however, are often strongly dependent on the original topography, obscuring the relationship with the ELA. Additionally, cirques are erosional features that cannot be assigned to individual glacial episodes (Benn and Lehmkuhl, 2000). The MELM method is also based on geomorphologic considerations. It assumes the minimum value for the ELA is the maximum elevation of the lateral moraines deposited by a glacier. General glacier kinematics supports this hypothesis, as glaciers will only deposit debris below the ELA (Cuffey and Paterson, 2010). Glaciers in steady state for a sufficiently long period of time should therefore develop lateral moraines sufficiently consistent to place a lower bound on the ELA. This lower bound, however, can be significantly below the true ELA, and the difference between the lower bound and the true ELA is highly variable from one glacier to the next, making it extremely difficult to

quantify. Additionally, such features are exposed to erosional events that often obscure the true maximum elevation of these moraines. The MELM method, therefore, can provide a useful rough estimate of past ELA, but there are few to no analytical validations of the accuracy of the results.

The balance ratio (BR) method is one of the more complex and physically-based ELA reconstruction methods commonly used. The BR method takes into account valley hypsometry and the ratio between gradients in ablation and accumulation (Furbish and Andrews, 1984). Where such data is available and reasonably constrained, this method is considered the most rigorous and accurate of those discussed, taking into account gradients that directly affect the glacier mass balance and, by extension, the ELA (Benn and Lehmkuhl, 2000). The BR method, however, requires initial assumptions regarding the climate in question. Due to these a priori requirements of climatic conditions (i.e. the accumulation and ablation gradients), this method is more difficult to apply to paleoclimate reconstructions without the risk of circular arguments.

All of these methods, although useful in certain circumstances, highlight the need for additional progress to help better constrain ELA estimates in a robust, self-consistent manner, while still requiring minimum inputs. Such a method, combined with tight age constraints, would allow for more accurate, temporally precise comparisons of shifts in climate across regions. This in turn would help to elucidate the primary factors involved in such changes. Here we detail a new ELA model intended specifically to address these concerns, incorporating contributions from the bed topography and areal distribution of a glacier, along with estimates of glacier ice thickness. This new model is largely derived from a simple linear glacier-length model proposed by Oerlemans (2011), with modifications specific to quantifying ELAs and ELA changes. We furthermore provide model uncertainty estimates based on standard Monte Carlo simulations,

also taking into account uncertainty in model input data. As a test of the model's accuracy, we compare the model results for present-day glaciers in the Swiss Alps both with previously published estimates of the ELAs and with the modern summertime snowline in the region. We then apply this model to three Egesen Stage glacier moraine sequences in Switzerland, with newly obtained surface exposure ages correlating these sequences to the Younger Dryas cold interval. Using a simple temperature index model, we estimate the necessary change in temperature to drive this change in ELA relative to the modern day. Such results yield additional evidence concerning the primary drivers of the Younger Dryas climate event in the Swiss Alps.

### 3 METHODOLOGY

A balance must be struck between the applicability and ease of use of a model, and the factors and physics a model can readily incorporate. This research presents a method to reconstruct ELA estimates based largely on physical relationships, while still requiring minimal data input. This necessarily requires numerous simplifying assumptions, which ignore some details pertinent to individual glaciers. Such details are significant for some applications (e.g. dynamic modeling of glacier response, higher order surface energy and mass balance modeling), and other methods would be better suited to these circumstances. The proposed model is specifically intended for snow-fed, clean ice, temperate glaciers with relatively simple bed geometries, and caution should be used in applications beyond these boundaries. This ELA model is similar in simplicity to such methods as THAR or AAR methods, but more physically based rather than relying purely on empirical correlations. It therefore should be more readily and generally applicable without regard for tuning to regional climate conditions.

Physical relationships give direct applicability and robustness to these models over statistical models of similar resolution through better accounting of intrinsic differences between glacier systems. AAR, THAR, or other similar statistical ELA models often fail to account for differences in glacier bed elevation, ice thickness, profile shape, etc. which have measurable effects on the overall ELA of a glacier. Furthermore, although all models have certain limits outside of which they are invalid, statistical models rarely include indications of when a particular application lies outside these bounds. The ELA model presented here, by accounting for differences in physical characteristics, yields diagnostic results useful in determining how well the model captures different aspects of glacier characteristics, therefore providing validation of the applicability to a specific glacier. These attributes allow for more accurate results and greater applicability with increased confidence.

The ELA model provides analytical constraints on the error associated with model outputs. Such uncertainties help determine the significance and reliability of results, and are unfortunately not always adequately accounted for in paleoclimate research (Tarasov, 2012). Uncertainty estimates in this study are calculated based on Monte Carlo simulations of bootstrapped residuals of the input parameters. These uncertainties give insight into the range of plausible ELA values based on both uncertainty of input parameters and the ability of the model assumptions to accurately represent those inputs. Comparisons of model results for modern Swiss glaciers with both mass balance studies and multi-year mean summer snow line altitudes provide further validation for model accuracy.

### 3.1 ELA model

The fundamental basis of the ELA model is an integrated balance equation (Equation 1) for steady-state glaciers, adapted from Oerlemans (2011),

$$B_n = \int_0^L b dx = \beta \int_0^L [w(x) \cdot (H(x) + z(x) - ELA)] dx \quad \text{Equation 1}$$

Where  $B_n$  is the total net balance,  $x$  is the distance down glacier,  $b$  is the specific balance rate at  $x$ ,  $L$  is the glacier length,  $\beta$  is the balance gradient,  $w(x)$  is the glacier width at  $x$ ,  $H(x)$  the ice thickness at  $x$ ,  $z(x)$  represents the valley topography, and ELA is the equilibrium line altitude. In steady state conditions (like we assume for glaciers with well-developed moraine sequences), the total net balance is zero. Equation 1 can then be rearranged to solve for the ELA (Equation 2), where the balance gradient divides out,

$$ELA = \frac{\int_0^L w(x)H(x)dx + \int_0^L w(x)z(x)dx}{\int_0^L w(x)dx} \quad \text{Equation 2}$$

We then estimate each of the three components (ice thickness, glacier width, and bed elevation) along the length of the glacier. Methods for the estimation of each of these parameters are detailed below.

#### 3.1.1 Glacier bed modeling

Sources for valley elevation measurements in this study are DEMs from Swisstopo and LP DAAC ASTER GDEM databases, but other methods for obtaining elevation measurements (other remote sensing data, field surveying, etc.) are equally feasible. Bed topography measurements follow a representative 1D line along the glacier profile, typically taken down the center of the glacier. We then estimate  $z(x)$  from a best-fit two-term exponential curve of this 1D profile line (Equation 3), where  $a$ ,  $b$ ,  $c$ , and  $d$  are fitting coefficients determined by the model.

$$z(x) = ae^{bx} + ce^{dx}$$

Equation 3

Approximately ten quasi-equally spaced points along the length of the glacier are often sufficient to constrain the exponential curve, though the optimum number depends on the length and complexity of the bed topography. This two-term exponential estimate is best suited for valleys with relatively simple bed topographies. Caution should be used when applying this method to glacier beds with more complex bed features, such as steep cliffs or over deepenings, as these are not always readily captured in the model (Figure 1).

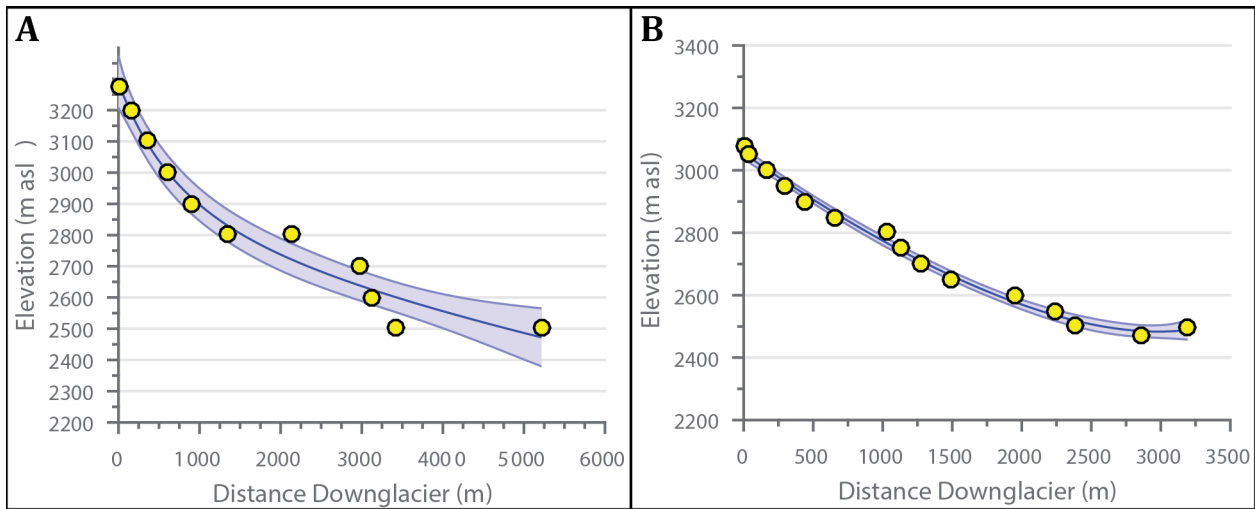


*Figure 1. Plots comparing model performance for glacier beds of varying complexity. Yellow circles are measured bed elevations. Black lines are the modeled bed topography, while the blue shading represents  $\pm 2$  standard deviations. Plot A shows the results for the Gries Glacier, and B shows results for the Silvretta Glacier. Note the pronounced over deepening in A, which is less accurately accounted for in the model results. This contrasts with the Silvretta Glacier on the right, where the modeled bed matches the measured values more closely.*

### 3.1.2 Glacier width modeling

Glacier width measurements in this study are taken from aerial and satellite images from Swisstopo, LANDAT, DigitalGlobe, and GeoImage Austria databases. Due to the high diversity in glacier shape/geometry, estimating the plan-view profile of the glacier in a consistent yet simple manner is difficult. Additionally, accurately constraining the width of the accumulation

area for paleoglaciers presents further challenges, due to a lack of preserved moraines or other features delineating glacier boundaries in these areas. To best cope with these issues, we estimate glacier width using an exponential equation of the same form as Oerlemans (2011) (Equation 4). We then use a least squares nonlinear curve fit to optimize the width estimation. The initial starting parameters are the minimum width of the glacier at the toe ( $w_0$ ), maximum glacier width in the accumulation zone ( $w_{max}$ ), the distance down glacier (x), and the distance down glacier to the point of maximum width ( $L_{Wmax}$ ).

$$w(x) = w_0 + \frac{(w_{max}-w_0)}{L_{Wmax}} xe^{1-\frac{x}{L_{Wmax}}} \quad \text{Equation 4}$$

This produces an exponential curve, following the general shape of many glaciers. The model then modifies these three initial values ( $w_0$ ,  $w_{max}$ , and  $L_{Wmax}$ ) to reach an optimal fit with the input width values for a specific glacier (Figure 2).

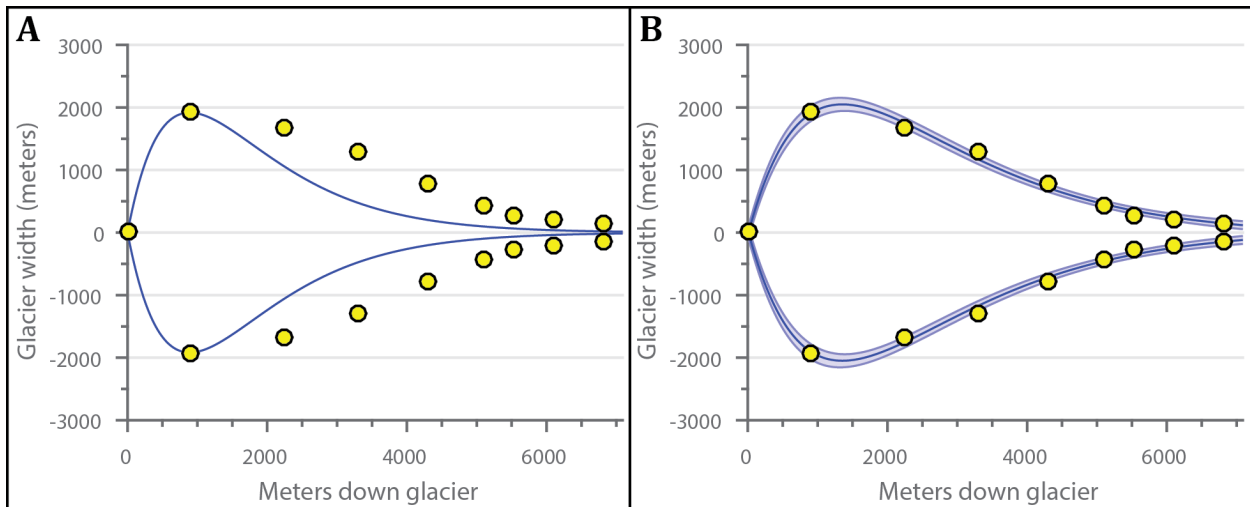


*Figure 2. Comparison of model width initial guess vs. optimal fit. Panel A shows the initial guess using Equation 4, while Panel B shows model width with optimized parameters of Equation 4. Yellow circles are measured bed elevations. Black lines are the modeled bed topography, while the blue shading represents  $\pm 2$  standard deviations. Although A captures the general shape and trend of the glacier, B matches measured values much more closely.*

### 3.1.3 Ice thickness modeling

To first order, the thickness of a glacier depends largely on the slope and shear stress at the bed (Cuffey and Paterson, 2010). The simplest equation to approximate ice thickness is therefore

$$H = \frac{\tau}{\rho g \sin \theta} \quad \text{Equation 5}$$

where  $H$  is the ice thickness (m),  $\tau$  is the basal shear stress (Pa),  $\rho$  is the ice density ( $\text{kg/m}^3$ ),  $g$  is acceleration due to gravity ( $\text{m/s}^2$ ), and  $\theta$  is the angle at the bed interface (Cuffey and Patterson, 2010). In areas with shallow slopes ( $\theta$  close to 0), however, this equation leads to ice thickness unrealistically approaching infinity. Oerlemans (2011) demonstrates a square root relation between length and ice thickness (assuming perfect plasticity), which we incorporate into our estimates in order to address this issue (Equation 6).

$$H_m = \frac{2}{3} \sqrt{\frac{\tau L}{\rho g(1+\sin \theta)}} \quad \text{Equation 6}$$

This equation, however, gives the mean ice thickness ( $H_m$ ) for the glacier, rather than discrete values along its length. To model ice thickness profiles, we assume a parabolic distribution (true of a perfectly plastic glacier on a flat bed) around the mean ice thickness. Ice density is assumed to be  $917 \text{ kg/m}^3$  and the gravitational acceleration is set at  $9.8 \text{ m/s}^2$ . The basal shear stress ( $\tau$ ) is assumed to scale with ice thickness, following the relationship presented in Haeberli and Hoelzle (1995), where  $\Delta z$  is the difference between the minimum and maximum bed elevation (Equation 7).

$$\begin{aligned} \tau &= 150 \text{ kPa} & \Delta z &\geq 1600 \text{ m} \\ \tau &= 3 \Delta z & \Delta z &\leq 500 \text{ m} \\ \tau &= 0.005 + 1.598 \Delta z - 0.435 \Delta z^2 & 500 \text{ m} &\leq \Delta z \leq 1600 \text{ m} \end{aligned} \quad \text{Equation 7}$$

### 3.2 Monte Carlo Simulations

We perform Monte Carlo simulations to capture the distribution of plausible ELAs for a given glacier. Such estimation of uncertainty is important to adequately compare the significance of results, particularly if attempting to compare results from differing methodologies or between regions. Monte Carlo methods are widely used to characterize the range and distribution in the outputs of models for physical systems (e.g. Tarasov et al., 2012; Colgan et. al., 2012; Kuczera and Parent, 1998). Such techniques are well suited to provide bounds of uncertainty, particularly within inter-related and multivariable systems with numerous degrees of freedom (Kroese et. al., 2011; Colgan et. al., 2012). Indeed, several studies investigating glacier mass and energy balances use similar Monte Carlo methods for uncertainty estimation (Mölg et al, 2012; Machguth et al, 2008; Konz and Seibert, 2010). In our approach, each simulation includes bootstrapping with replacement techniques to assess the uncertainty in model estimation. Bootstrapping is a resampling scheme often used for significance testing of multivariate data sets (Trauth, 2010). We use it here to determine how accurately we model our input parameters, and we further include any known errors in those parameters (bed elevation, glacier width, and mean basal shear stress), assuming Gaussian distributions in these error values. Each model run consists of 1,500 iterations in order to approximate a continuous distribution in plausible ELA values.

### 3.3 ELA Estimates from Snowlines

The primary goal of this ELA model is to reconstruct past climate, particularly relative to modern day. This obviously necessitates an estimate of the present day ELA in the particular region in question for comparison to the paleo-ELA. For currently glacierized valleys, the ELA

model can be applied to both modern and paleo extents of the glacier, the technique we apply wherever possible. When no glacier is currently present, the regional end-of-summer snowline in an area can often serve as an approximation of the ELA for a glacier (Cuffey and Paterson, 2010). To obtain this snowline estimate, we use a supervised maximum likelihood classification scheme in a GIS environment, similar to remote sensing methods used in previous studies (e.g. Rabatel et. al., 2012; McFadden et. al., 2011; Bronge and Bronge, 2010; etc.). The classification distinguishes between snow and ice, creating polygons for each. Training sets of ~10 polygons for each class were used to define the automated classification. In order to estimate the analytical error in this method, we look at both the minimum elevation of snow class polygons and the maximum elevation of ice class polygons. In theory, both these values should be equal to the snowline, but in practice some offset typically exists between the two values. We define the difference between the iceline and the snowline as the analytical error of the annual estimate. Such methodology also gives two estimates of the snowline for each year, further constraining the uncertainty in the measurement.

Elevation data are ASTER global DEMs, with mean vertical resolution of 30 m and horizontal resolution of 20 m. Images used for the classification scheme are composite rasters of Bands 1 (0.45-0.52  $\mu\text{m}$ ), 4 (0.76-0.90  $\mu\text{m}$ ), and 5 (1.55-1.75  $\mu\text{m}$ ) of the LANDSAT 5 Thematic Mapping (TM) dataset. Images used have 10% or less cloud cover, and span the end of the ablation season (late August-early September) during the years 2006-2011, a timespan similar to ELA estimates derived from snowline elevations in Spiess et. al. (2015). Individual locations occasionally have gaps in this time span due to satellite maintenance or other issues.

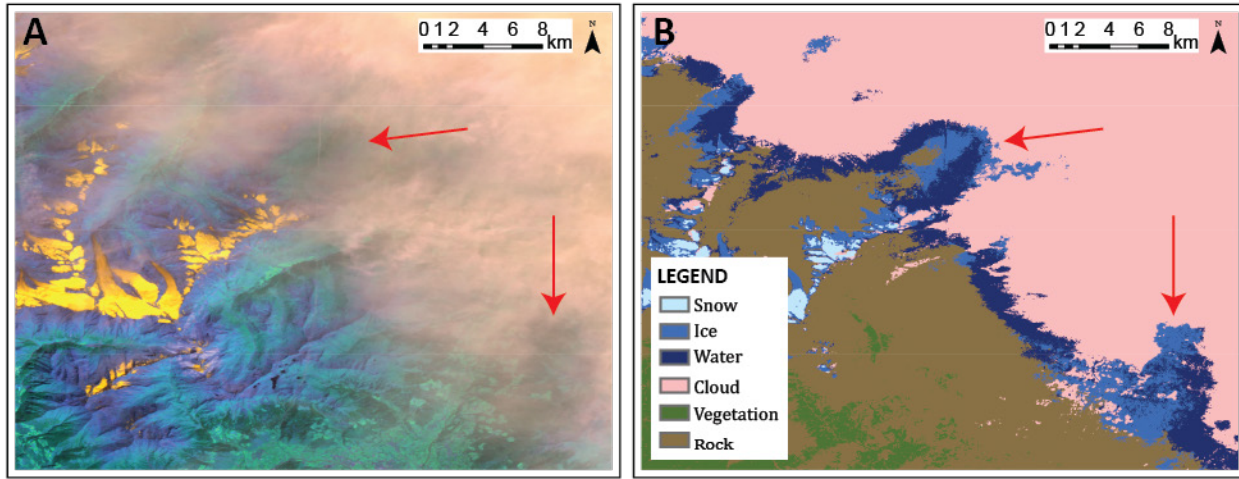


*Figure 3. Example of the misclassification of cloud cover as ice. Images are located near the Silvretta Glacier (see Figure 7). Panel A is a LANSAT TM 5 image while Panel B shows the corresponding classes from the unsupervised raster classification. The red arrows indicate areas where significant portions of cloud (pink class) are incorrectly classified as ice (mid-blue class). Because this misrepresentation does not have any systematic grouping of elevations, it is difficult to attribute ice polygon outliers to this cause. In an attempt to avoid this bias, we selected only LANSAT images with minimal cloud cover. Data available from the U.S. Geological Survey and the NASA Land Processes Distributed Active Archive Center.*

In addition, each annual dataset was manually inspected for systemic incorrect classifications and, where possible to differentiate, the incorrect values were removed. Such errors were commonly the misclassification of water bodies or cloud cover as ice (Figures 3-5). Typical years contain thousands to tens of thousands of measurements within a study area (approximately 2,000 km<sup>2</sup>).

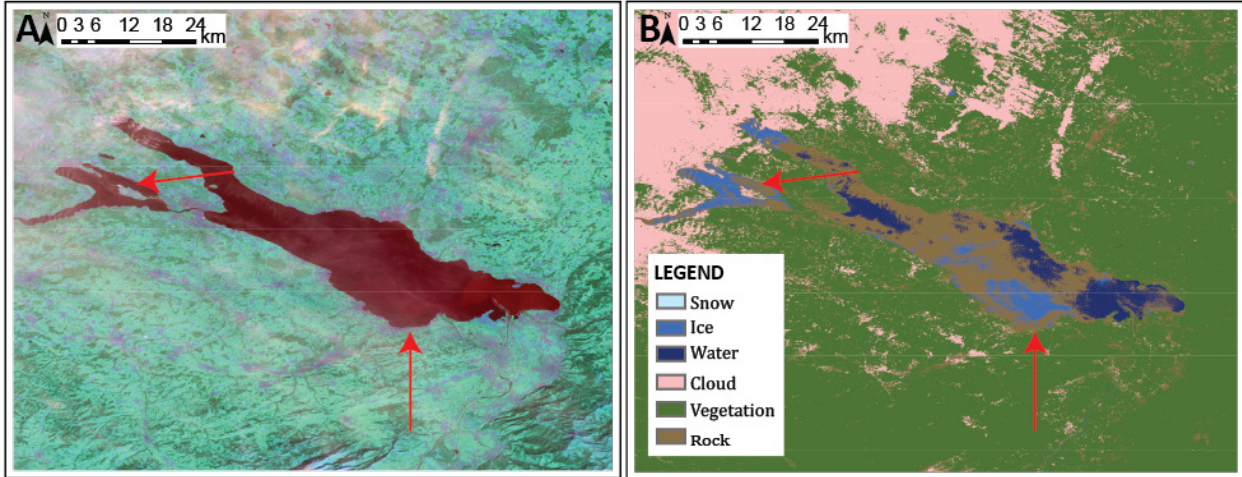


*Figure 4. Example of misclassification of water as ice. Images are approximately 30 km north of images in Figure 3. The red arrows indicate areas where portions of water (dark blue class) are incorrectly classified as ice (mid blue class). Unlike the cloud misclassification, elevations from a continuous body of water can often be identified and manually removed post classification (see Figure 5). Data available from the U.S. Geological Survey and the NASA Land Processes Distributed Active Archive Center.*

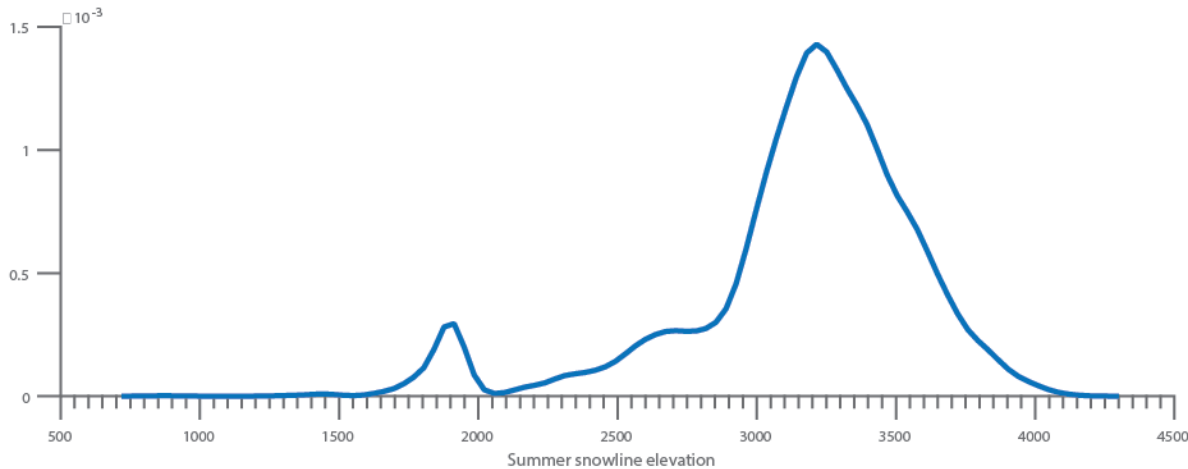


*Figure 5. Probability density function of a snowline distribution that includes a misclassified water body (Figure 4). The anomalous lower spike in the distribution (~1900 m a.s.l.) represents mislabeled water polygons from the nearby lake. A quick manual inspection of the original LANDSAT and classified images can confirm such anomalies as outliers, which can then be removed from snowline calculations.*

Such methodology can involve complex uncertainties beyond the scope of this paper, and we make no attempt to fully quantify these more complex associations. We instead present conservative estimates of the uncertainty of the snowline measurements based on elementary statistics. The mean regional snowline is calculated from the mean of the median values of both

the snow class and ice class estimates from each year in a region. The median value was selected due to non-Gaussian distributions in several of these annual data sets. We assume the mean of these median values approximates the true regional snowline (i.e. the ELA). Using the mean of the annual estimates (rather than the mean of bulk measurements) also avoids weight biasing the final result towards years with greater snow cover (i.e. more data points in those years). Margins of error (95% confidence intervals) are calculated using t-score statistics of the two median values of each year. Additionally, we use Monte Carlo simulations (1,500 iterations) to incorporate the estimated mean analytical error at each site.

### *3.4 Temperature and precipitation reconstructions*

Reconstructing changes in the ELA provides a self-consistent means to evaluate the magnitude of glacier changes over space and time. Additionally, the changes in ELA are the result of changes in mass balance, and are therefore an excellent proxy for changes in the climate. Here, we avoid assumptions about the ELA-climate relationship by first reconstructing the changes in accumulation and ablation represented by the ELA change. We use a first-order Taylor series expansion of the glacial-meteorological model (e.g., Kerschner, 2005; Rupper et al., 2009) to relate the change in ELA to a change in accumulation and ablation (Equation 8).

$$\Delta A_c = \Delta A_b + \frac{\partial A_b}{\partial z} \Delta ELA \quad \text{Equation 8}$$

Where  $\Delta A_c$  is the change in accumulation ( $\text{kg/m}^2$ ),  $\Delta A_b$  is the change in ablation ( $\text{kg/m}^2$ ), and  $\frac{\partial A_b}{\partial z}$  is the gradient in ablation with altitude. Equation 8 assumes no gradient in accumulation with elevation, valid for elevation changes of a few hundred meters or less. We use a value of -4.0 ( $\text{kg/m}^2/\text{m}$ ) ± 1.0 for the ablation gradient, a range appropriate for many temperate glaciers from the modern Alps and similar locations (Kuhn, 1984; Ivy-Och et. al., 2006; Kerschner 2004). This

value is further supported by estimations of ablation gradients directly from ablation model outputs for glaciers in this study and modern climate data, which fall within the above range of prescribed uncertainty.

To find the maximum possible change in accumulation, we assume the change in ELA results solely from changes in accumulation, setting  $\Delta A_b$  to zero. We use the reciprocal approach to find the maximum change in ablation from the calculated  $\Delta$ ELA. We then use a simple positive degree-day (PDD) model to derive an upper bound for the change in temperature required to drive this change in ablation, assuming all ablation occurs as melt (an accurate approximation for temperate glaciers, like those in the Alps).

For a simple positive degree-day model, the total melt relates to the above-freezing air temperature summed over a period of time intervals (expressed as positive degree-days) multiplied by a proportionality factor, called the degree-day factor (DDF),

$$Melt = DDF \cdot PDD \quad \text{Equation 9}$$

$$PDD = \sum_{t=1}^n T^+ \cdot \Delta t \quad \text{Equation 10}$$

where PDD are positive degree-days,  $T^+$  are air temperatures above freezing and  $\Delta t$  is the time interval (in this case days). Due to few required input values and similar characteristics, temperature index models are the most widely used method for modeling the melting of snow and ice (Hock, 2005). Despite the rather simple assumptions in temperature index models over more complete surface energy and mass balance approaches, strong correlations between air temperature and various energy components (shortwave radiation, longwave flux, and turbulent heat exchange to name a few) enable PDD models to often perform on par with SEMB models in many circumstances (Hock, 2005; Cuffey and Paterson, 2010).

Temperature index models are statistical rather than physical models. They therefore are less generally applicable than more physically based models, and certain parameters (i.e. the DDF) must be tuned empirically. Because it represents the combined contribution of many different energy components, DDFs can be highly variable in both space and time. We assume a DDF of  $6.0 \text{ mm/PDD} \pm 2.0 \text{ mm/PDD}$ , a range supported by numerous other studies on glaciers in the Swiss Alps and other climatically similar regions (Braithwaite and Zhang, 2000; Hocke, 2003; Braithwaite, 1995). This range spreads dirty ice to clean firn (Cuffey and Paterson, 2011), and is likely to capture the spread in DDFs at the ELA under paleoclimate settings as well. We will focus future work on utilizing a more physically-based approach (e.g., SEMB models). For this study, however, we use Monte Carlo simulations with a reasonable distribution in DDFs and ablation gradients to estimate the likely change in air temperatures necessary to produce the change in ablation predicted using Equation 8.

Using the change in ablation calculated from Equation 8, we then iteratively solve for the mean annual temperature corresponding to a change in PDDs from the modern day value using Equation 11.

$$T_a = \bar{T} - \frac{1}{2}(T_{max} - T_{min}) \cdot \cos(2\pi\omega t) \quad \text{Equation 11}$$

Here,  $T_a$  is the air temperature at a given time  $t$ ,  $\bar{T}$  is the mean annual air temperature,  $T_{max}$  and  $T_{min}$  are the maximum and minimum air temperatures throughout the year, and  $\omega$  is the period of the seasonal cycle (in our case  $\frac{1}{365 \text{ days}}$ ). Equation 11 accurately captures the seasonal changes in monthly surface air temperatures in south central Switzerland from 1981 to 2010 (Figure 6). For temperature reconstructions, we assume the amplitude of the seasonal temperature cycle varies between  $\pm 10\%$  of the present-day value.

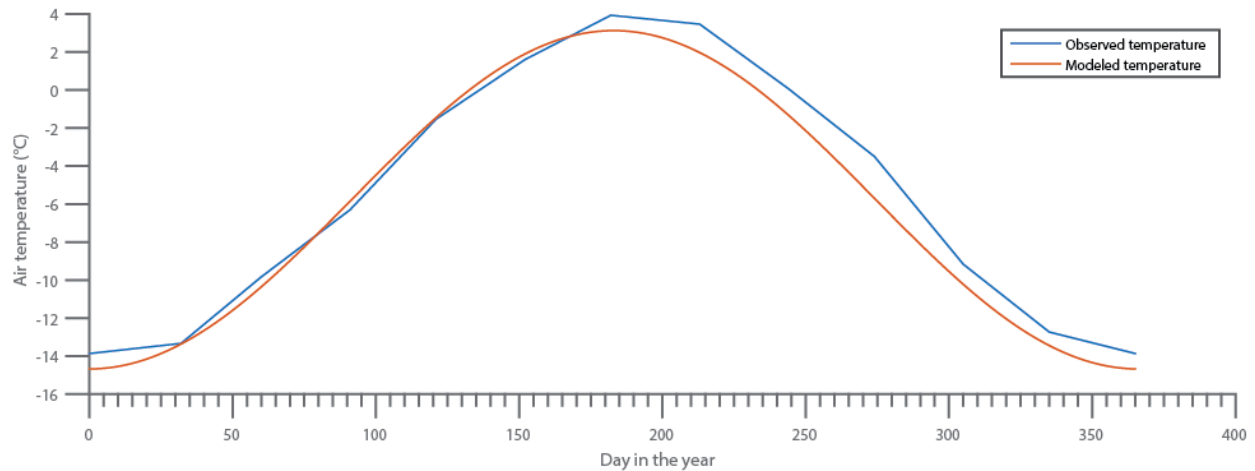


*Figure 6. Comparison of modeled temperature throughout the year (red) and actual observed average monthly temperature in south central Switzerland from 1981-2010 (blue). Equation 11 provides an excellent fit to the observed data. Because this model reconstructs a change in air temperature, the minor areas of offset between the modeled and observed temperatures should not significantly affect the results. Additionally, such discrepancies fall within the assumed error of  $\pm 10\%$  in the seasonal cycle amplitude.*

Modern temperature and precipitation data is provided through SwissMeteo. For this study, we define present-day temperature and precipitation using monthly mean 2 m air temperatures averaged from 1981 to 2010. For sites where no weather station is present, we average temperatures from nearby stations (adjusted to the present day ELA using a locally defined temperature lapse rate of  $5.4^{\circ}\text{C}/\text{km}$  based on temperature data from SwissMeteo stations at Samedan, Chur, and Piz Corvastch) to approximate the temperature and precipitation at that site. Annual solid precipitation (water equivalent) is estimated through summation of monthly precipitation values for months with temperatures below freezing.

These temperature/precipitation estimates necessarily include many more assumptions and simplifications than the ELA reconstructions detailed earlier. These include assumptions regarding the local temperature lapse rate, ablation gradient, degree-day factor, and the magnitude of the seasonal cycle, in addition to all the uncertainties already inherent in the ELA model. We base many of these assumptions off of modern values and characteristics of the

studied region, but without guarantee such assumptions hold for earlier time periods. We again utilize Monte Carlo simulations to incorporate uncertainties associated with each input parameter into the quantification of errors in our climate reconstructions. The summation of these errors makes the uncertainties in the climate reconstructions larger than that of the ELA model. Use of the PDD model, however, allows for valuable comparisons of temperature and precipitation reconstructions from sources independent of the glacial record (e.g., fossil pollen records, paleo-lake records, speleothems).

## 4 RESULTS

We first validate the new ELA model for four present-day glaciers, demonstrating its performance and discussing potential issues in its application. We then apply the ELA model to three Younger Dryas paleoglaciers, investigate discrepancies, and calculate Younger Dryas ELA depressions relative to modern day. Finally, we estimate the change in mean temperature needed to produce the observed  $\Delta$  ELA for a range of changes in precipitation.

### 4.1 *ELA model validation*

Before applying our proposed methodology to paleo-glaciers, we tested the modeled ELAs with independent ELA data. In particular, we chose 4 glaciers in the Swiss Alps based on their close proximity to our target paleoglaciers. These glaciers were also selected due to the availability of data requisite for a data-model comparison (including present-day ice thickness, bed topography beneath the present-day glacier, mass balance measurements, aerial photography and DEMs). The four test glaciers are the Gries Glacier, the Findel Glacier, the Rhone Glacier, and the Silvretta Glacier (Figure 7). These glaciers were further selected due to differences in

overall shape and extent, thereby providing a wide range of possible glacier geometries. Three of these glaciers (Gries, Silvretta, and Findel) have continuous multi-year mass balance measurements from stake networks compiled by the World Glacier Monitoring Service (WGMS), and therefore make for the most compelling comparisons. The Rhone Glacier has mass balance measurements from a handful of isolated years, providing a less certain, but still useful comparison to the model and other glaciers.

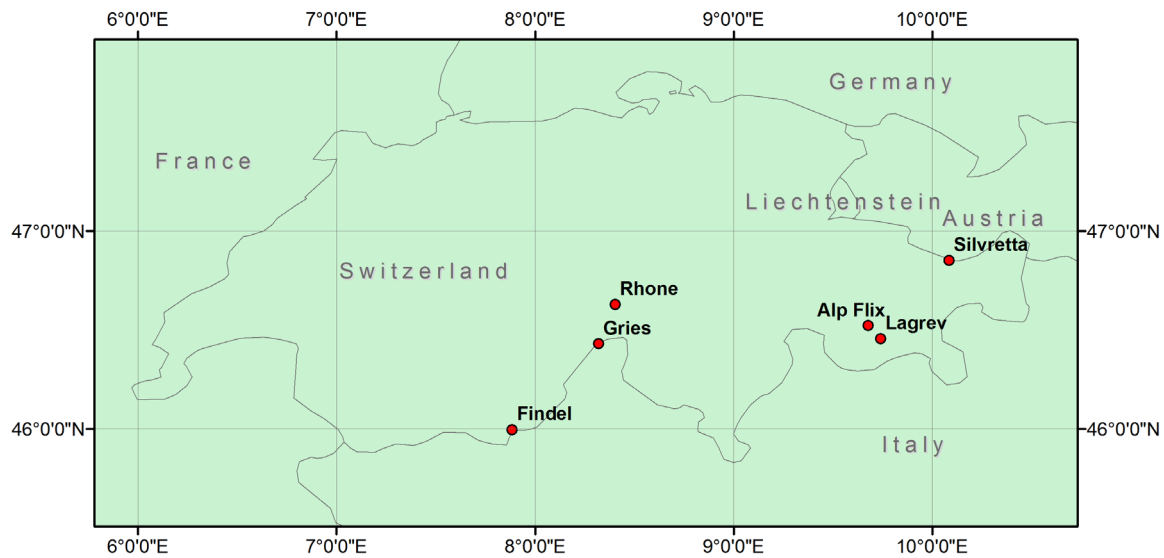


*Figure 7. Index map showing the locations of validation and paleoclimate reconstruction glaciers. Alp Flix and Lagrev are paleoglacier targets, while the rest are modern day glaciers used for validating the ELA model.*

#### 4.1.1 Data sources

We obtained width and overall length measurements for the 4 validation glaciers from aerial and satellite imagery. These data are summarized in Figure 8. Although exact margins of error for these data were not readily available, we assume an error of  $\pm 30$  m, a similar resolution to satellite images from NASA's LANDSAT 5 database. ASTER GDEM<sub>s</sub>, with a prescribed error of  $\pm 30$  m, provided ice surface elevations, which we use in combination with measurements

of bed topography to calculate ice thickness. Bed elevations are from modeled topographies in Farinotti et. al (2009) and Farinotti (2010), which they constrained using multiple GPR profiles and/or borehole depths for each glacier.

Mass balance and ELA measurements were acquired from the WGMS and a study by Zemp et. al., (2007). The Silvretta and Gries glaciers have the best-constrained mass balances with ~50 years of published data for each (PSFG, 1967; PSFG, 1973; PSFG, 1977; PSFG, 1985; WGMS, 1988; WGMS, 1993; WGMS 1998; WGMS 2005; WGMS 2008; WGMS 2012). In order to compare the current climatic ELA of these glaciers with our modeled ELA, we calculate the median mass balance ELA from the linearly detrended annual ELA values from 1960-2010 for both glaciers, with uncertainty calculated to the 95% confidence interval. The Findel Glacier has similarly well-constrained mass balance measurements from a glacier stake network, but with a much shorter record (2005-2010) which we use (also linearly detrended) to estimate the climatic ELA (WGMS, 2012). The Rhone Glacier does not have consistent year-to-year mass balance measurements. Instead, we take modeled steady-state ELA estimates from air temperature correlations (1971-1990) provided in Zemp et. al. (2007). These ELA estimates are constrained with the few years of available stake mass balances (mean  $r^2$  coefficient between balance ELA and air temperature-correlated ELA is 0.89). No uncertainty estimates were provided for the Rhone Glacier ELA. For consistency, we assume Gaussian uncertainties with bounds similar to the average uncertainty of the mass balances for the Silvretta, Gries, and Findel glaciers ( $\pm 48$  m).

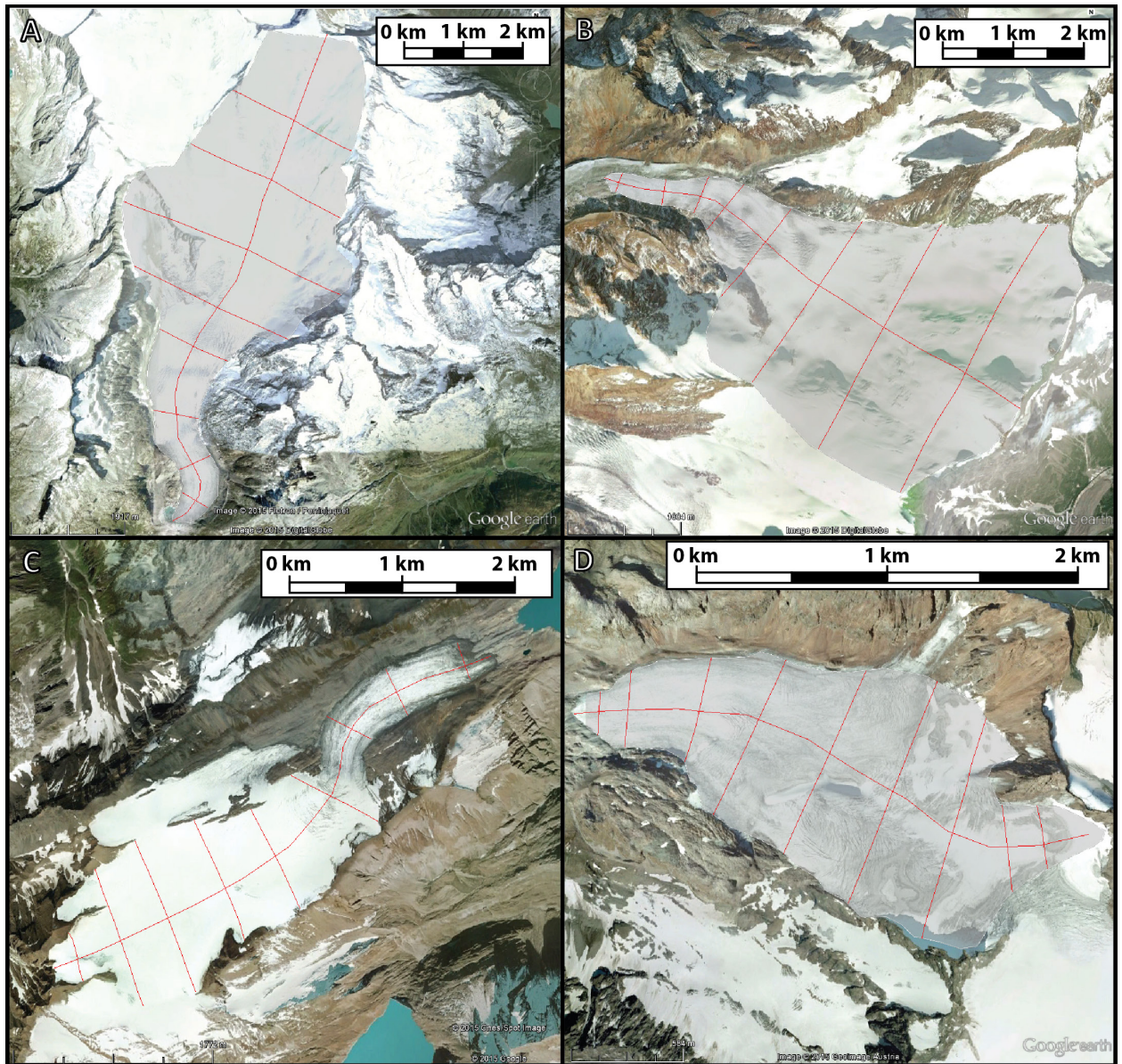


*Figure 8. Satellite and aerial photographs of the four test glaciers in the Alps: A) Rhone Glacier, B) Findel Glacier, C) Gries Glacier, and D) Silvretta Glacier. The red lines across each glacier denote the location of width measurements, while the line down the profile of each glacier denotes the location of the ice surface and length profiles. Data sources: A) 2015 Google, NASA, 2015 DigitalGlobe, 2015 Flotron/Perrinjaquet (Image date 8/31/2010). B) 2015 Google, 2015 DigitalGlobe (Image date 10/29/2009). C) 2015 Google, 2015 DigitalGlobe, 2015 Flotron/Perrinjaquet (Image date 8/31/2010). D) 2015 Google, 2015 GeoImage Austria (Image date 10/3/2009).*

#### 4.1.2 Model outputs

The model results, including bed topography, plan-profiles, ice thickness, and ELAs, are summarized in Figures 9-11. The modeled bed profiles all match measured values within estimated error (Figure 9). Because we compare model results against a single representative central profile line, minor departures from modeled topography likely represent local deviations in the measured central profile line. Exceptions to this include the overdeepened section apparent in the Gries Glacier (Figure 9C).

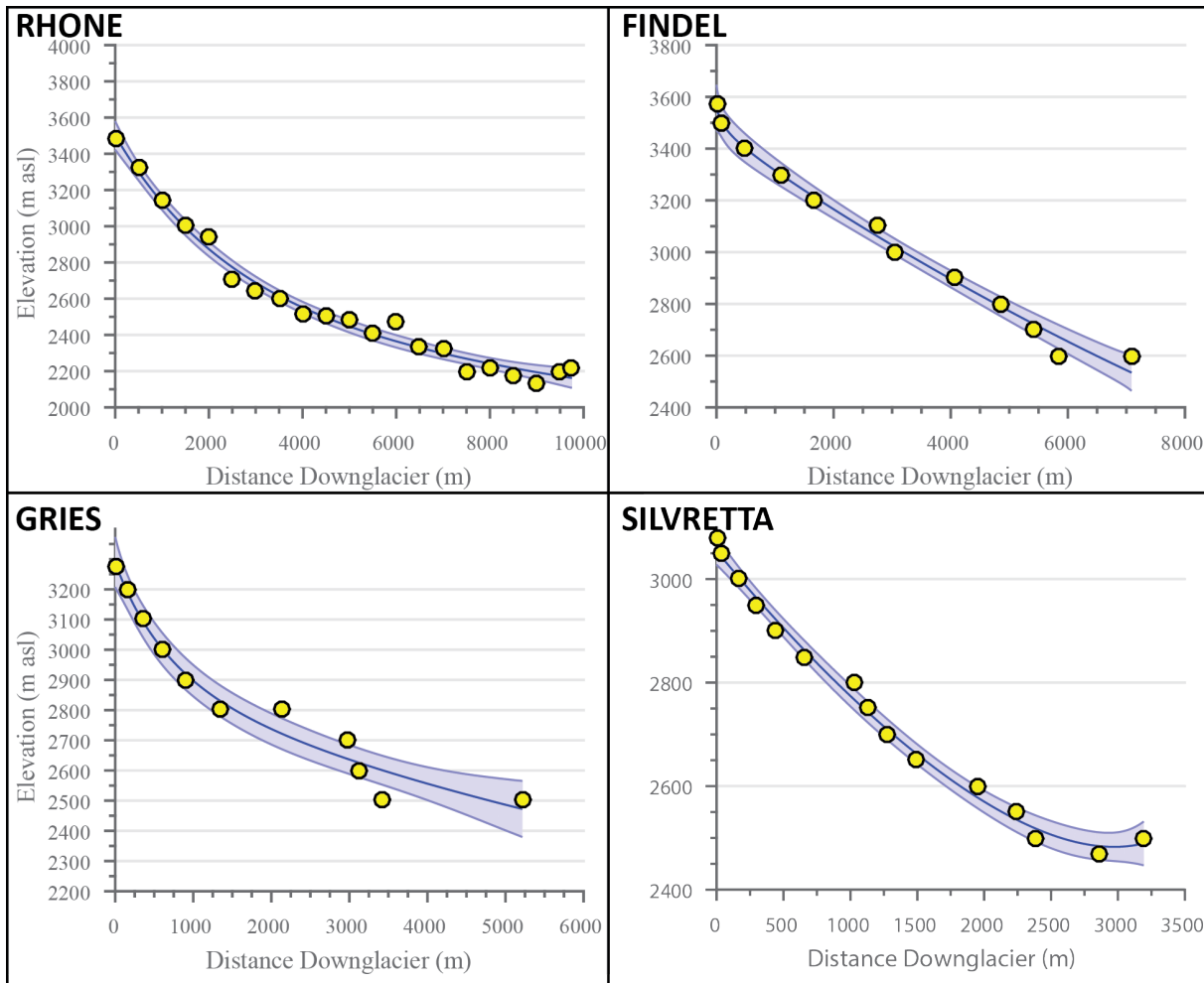


Figure 9. Bed elevation reconstructions for the four validation sites. Yellow circles denote independent bed elevation values, black lines represent the modeled bed profile, and blue shading represents model error ( $\pm 2$  standard deviations). The Gries Glacier (C) has an overdeepened section the model does not adequately account for, but overall the model sufficiently captures glacier bed profiles for all four glaciers. Topography data for Rhone (A) and Silvretta (D) obtained from Farinotti et. al. (2009). Topography data for Findel (B) and Gries (C) taken from Farinotti (2010).

Modeled glacier width results also closely match those recorded from aerial photography (Figure 10). The only noticeable exception to this is for the Rhone Glacier (A), with two clear outliers in the accumulation area. These may be related to difficulties in accurately defining the glacier boundaries in the accumulation area, or possibly due to characteristics (such as avalanching or tributary glaciers) not accounted for in the ELA model. Regardless, these inconsistencies should not significantly affect the ELA results, particularly when considering a change in ELA within the same valley.

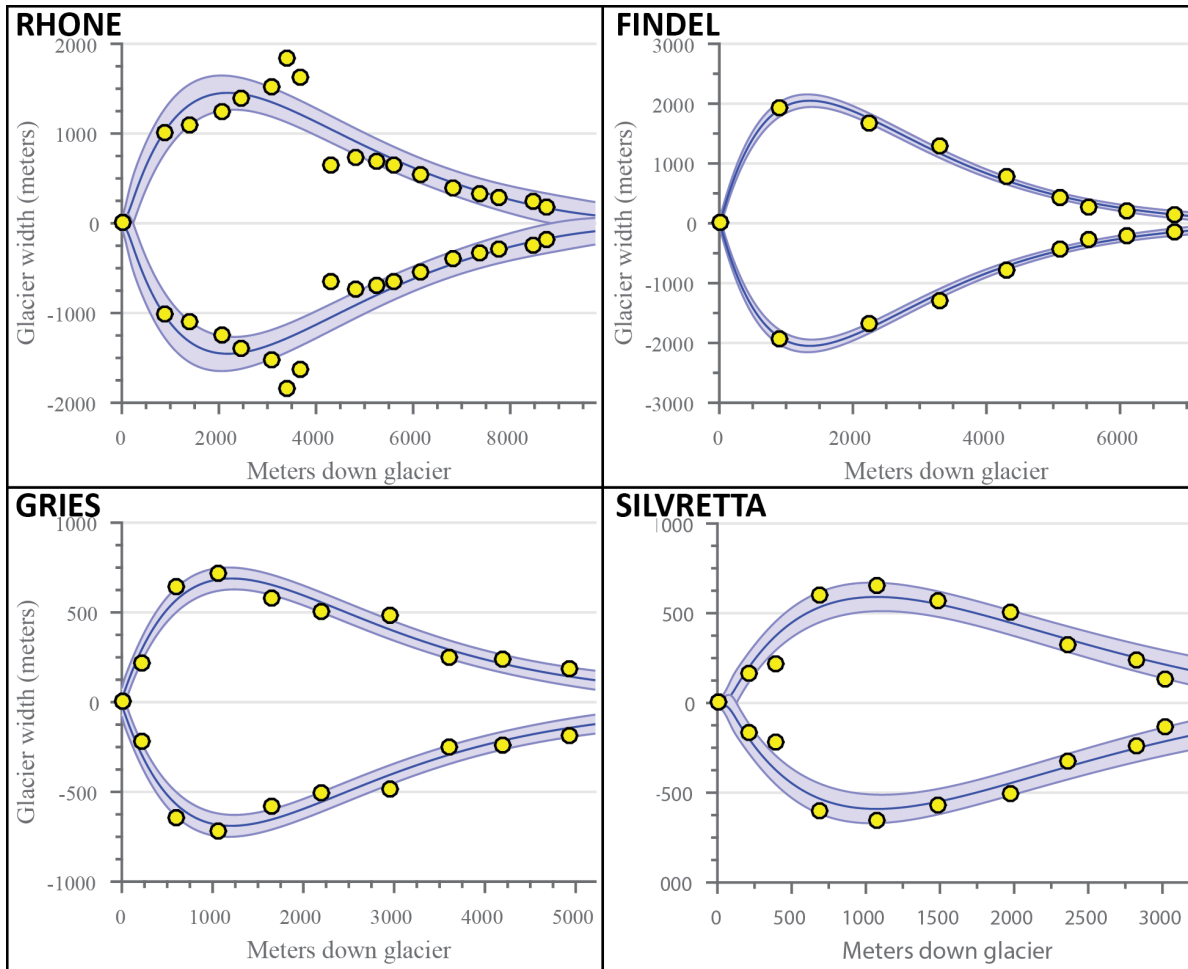


Figure 10. Glacier width modeling for the four validation sites. Compares the overall modeled areal profile (and modeled uncertainty) with discrete measured points of each glacier's width. Yellow circles denote width measurements for points on the glacier, black lines represent the modeled width profile, and blue shading represents model error ( $\pm 2$  standard deviations).

The reconstruction of the ice surface for each glacier is presented in Figure 11. Although the measured values most often fall within model bounds of uncertainty, individual points frequently deviate sharply from the model. Similar to the deviations in the bed topography, many of these deviations likely result from issues of localized effects at discrete points on the glacier and the simple approximation used for ice thickness (Equation 6). The ~30 m resolution of the images used for measuring the glacier surface leads to additional error. The exception to these explanations is Findel Glacier, which appears to be systemically overestimated by the model. Although isolating an exact reason for this overestimation is challenging, it may be related to ice flow dynamics and/or mass balance disequilibrium issues, neither of which are accounted for in this ELA model.

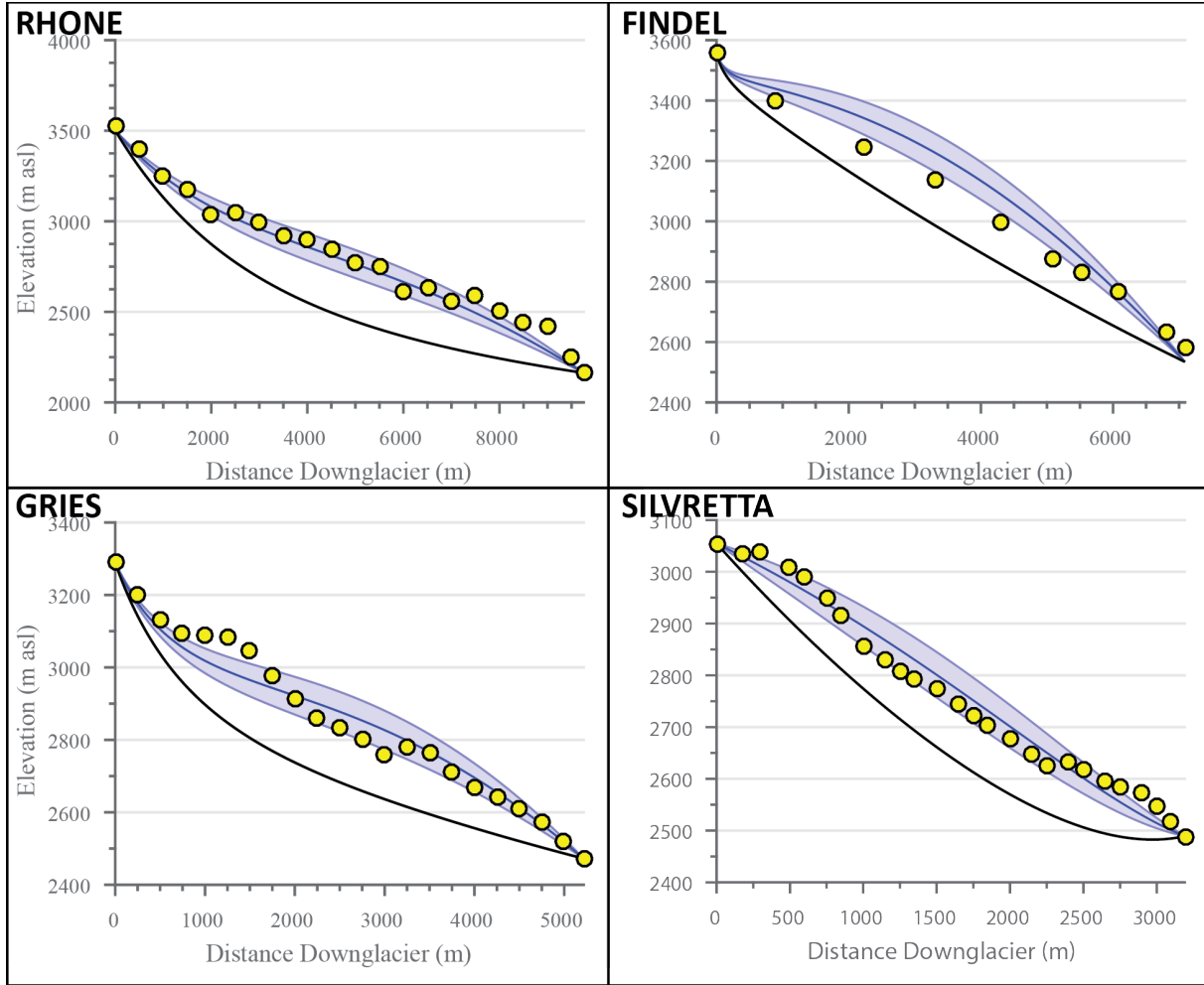
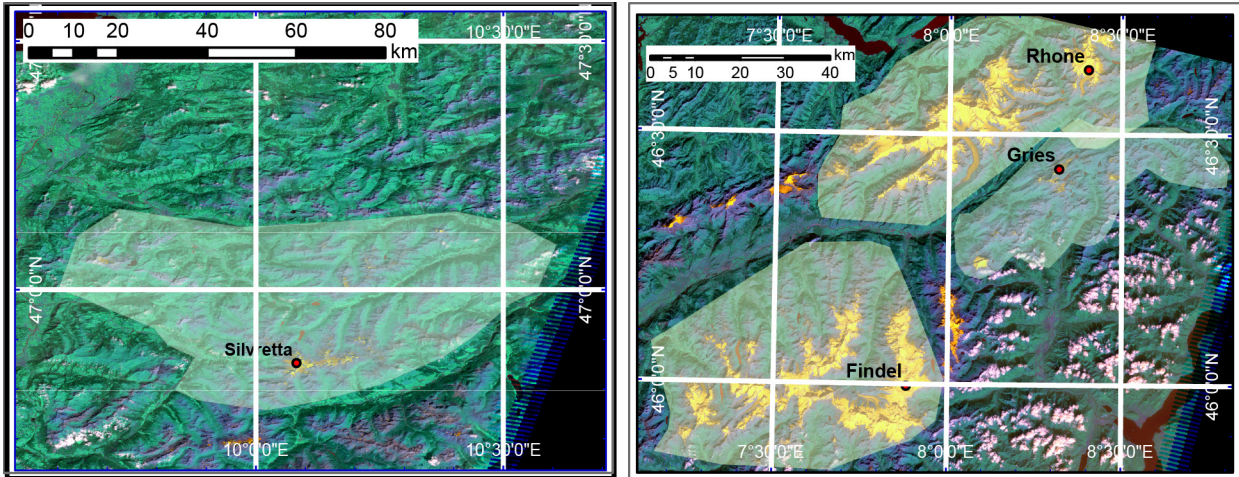


Figure 11. Modeled glacier ice surfaces for the four validation glaciers. Yellow circles denote independent ice elevation values, black lines represent the mean modeled bed topography (Figure 9), blue lines represent the modeled ice surface profile, and blue shading represents model error ( $\pm 2$  standard deviations). Uncertainty in ice thickness is determined by uncertainty in mean basal shear stress ( $\pm 35$  kPa). Ice surface elevations obtained from ASTER global DEMs (vertical resolution  $\pm 30$  m).

#### 4.1.3 Snowline ELA proxy results

Unfortunately, glaciers are not always present today in previously glaciated valleys of interest for paleoclimatic studies. Thus, an alternative approach must be used to calculate a  $\Delta$ ELA in those regions. The regionally-averaged snowline is one possible proxy for present-day ELAs that may be a useful approach in these situations. We test the validity of this approach by comparing regional snowline results using the supervised classification methodology to both the measured

and modeled ELAs at the four validation glaciers (Figure 7). Figure 12 shows the areas of interest for the calculations in representative LANDSAT images for the different glacierized regions. The snowline classification is performed over the time period 2006-2011. This represents the most recent coverage of the end of the ablation season from LANDSAT 5 data, with a duration similar to that of the shortest mass balance record (the Findel Glacier). This methodology often results in the largest estimated errors of the three ELA estimates used in this study. The 95% confidence interval (including mean analytical uncertainty) is typically between 100-200 m. These errors, although typically larger, are comparable to the uncertainty estimated using the ELA model. This ELA proxy, however, is the least physically connected to the actual ELA and provides less of a direct comparison than the ELA model in paleoclimate studies. The snowline method should therefore only be applied to areas where use of the ELA model is not valid or applicable, usually due to the absence of a present-day glacier to model. We demonstrate its use here to show its efficacy in comparison to other methods of ELA calculation and validate its use where other methods are not viable. Table 1 summarizes the results of the snowline analysis for the four glaciers, showing mean ELA estimates, mean analytical errors, and the total margins of error (95% confidence interval) for each.



*Figure 12. Map depicting areas over which summer snowline was calculated for the validation glaciers. The left image shows the calculation area for the Silvretta Glacier, while the right image shows the areas for the Findel, Gries, and Rhone glaciers. The location of each glacier is labeled in the figure. Images are raster composites of Bands 1, 4, and 5 of LANDSAT TM 5 images. Areal extent of each calculation area ~2,000 km<sup>2</sup>. Data available from the U.S. Geological Survey and the NASA Land Processes Distributed Active Archive Center.*

*Table 1. Summary of proxy ELA estimates from snowline analysis*

Glacier	Mean ELA (m a.s.l)	Mean Analytical Error (m a.s.l)	ELA margin of error (m a.s.l)
A. Rhone Glacier	2906	51	192
B. Findel Glacier	3306	29	125
C. Gries Glacier	2792	41	155
D. Silvretta Glacier	2851	43	82

#### 4.1.4 ELA comparisons

Figure 13 shows the ELA results for the four glaciers, and compares the model results to both the measured mass balance data and the snowline proxy data for each glacier. Table 2 likewise summarizes these results. Both the ELA model and the snowline analysis yield similar results to the mass balance measurements for all four validation sites. Likely sources of error to explain discrepancies between the results mostly involve more complex considerations not accounted for with the simple ELA model. For instance, more complex bed topographies, differences in shading/shielding by valley walls, debris cover, and accumulation through

avalanching can all affect the recorded ELA in mass balance measurements, none of which are included as considerations in the ELA model. In addition, the ELA model assumes steady-state conditions, where the annual mass balance is in equilibrium with the climate. This is a hypothetical condition often not true in reality. Glaciers typically have either an annual mass surplus or deficit, complicating comparisons of our results to mass balance ELA measurements, which incorporate these differences from steady state. This, however, is a limitation inherent to all ELA models. Finally, although the regional snowline can approximate the ELA of a glacier, local variations in topographic and climatic conditions cause discrepancies between the snowline and actual annual ELA of a glacier, at times by more than 100 m (Yuwei et. al., 2014). The observed discrepancies are some combination of these sources of error.

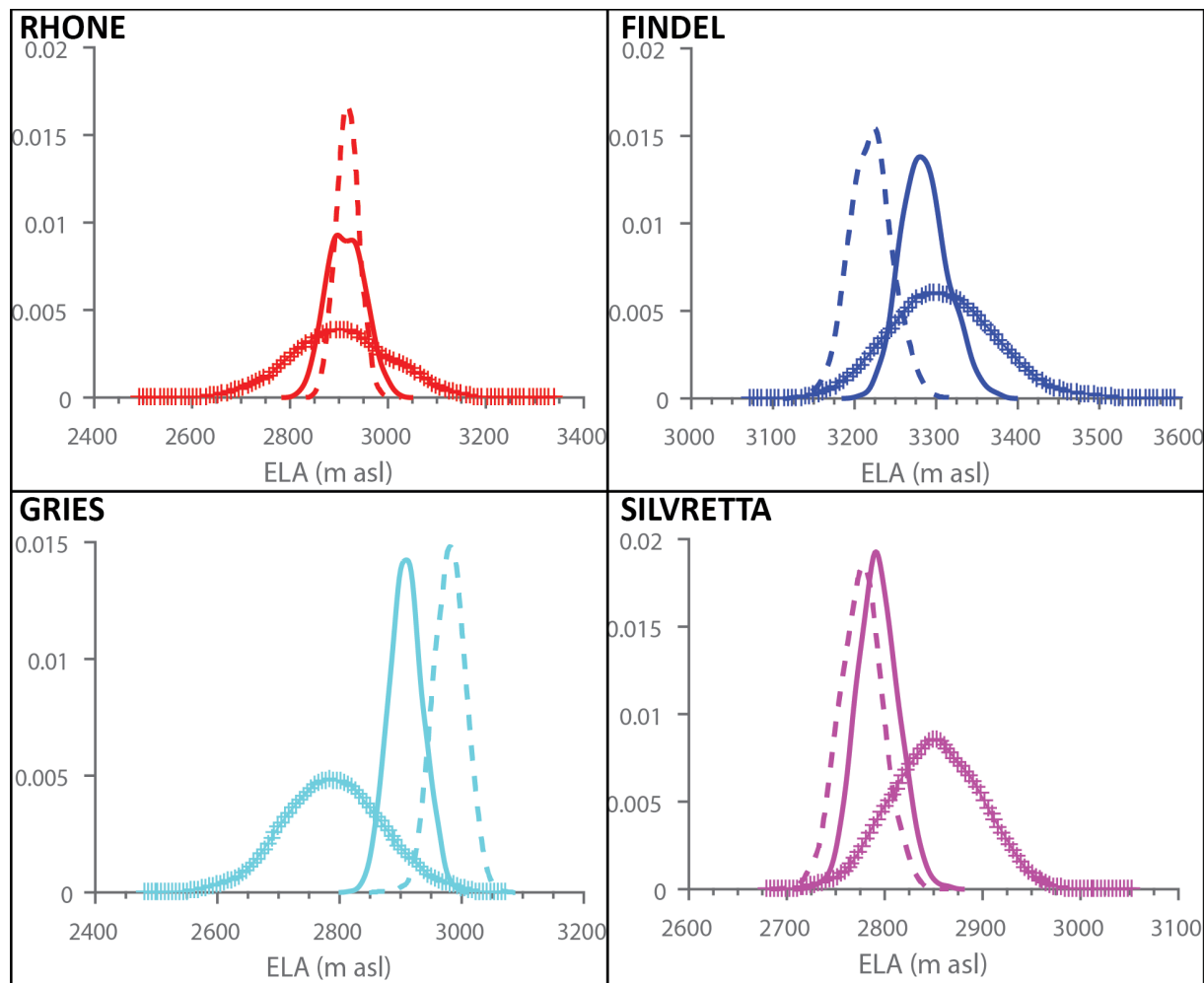


Figure 13. Probability density functions (PDF) for ELA results from the ELA model (solid lines), mass balance measurements (dashed lines), and snowline estimates (hashed lines). All three methods agree within error for all four validation sites.

*Table 2. ELA validation tests with associated error*

Glacier	ELA model	Margin of Error	Mass balance	Margin of Error	Snowline	Margin of Error
A. Rhone	2914 m	±75	*2918 m	±48	2906 m	±192
B. Findel	3284 m	±57	3220 m	±50	3306 m	±125
C. Gries	2909 m	±55	2980 m	±51	2792 m	±155
D. Silvretta	2792 m	±42	2777 m	±43	2851 m	±82

\*Rhone mass balance measurements from air temperature correlation (Zemp et. al., 2007) with mass balance constraints from isolated years

Regardless of the source of these errors, the results indicate the ELA model estimates the ELA within prescribed error relative to mass balance measurements for all four validation glaciers, as does the snowline proxy, albeit with less reliability. Such results lend strong support for the veracity of this ELA model for simple valley glaciers. In addition, many of the potential sources of error mentioned previously do not change significantly with time. By comparing ELA results between moraine sequences in the same glacial valley, the ELA model can implicitly account for these constant errors, thereby minimizing model biases. We therefore estimate  $\Delta$ ELA values from intra-valley moraine comparisons where possible, reserving snowline estimates only for glaciers where an ELA estimate from a modern glacier is not possible.

#### 4.2 Paleoglacier ELA reconstructions

The preceding tests validate the use of both the ELA model and snowline estimates for application to our target paleoglaciers in the Graubünden Alps (Figure 7). These targets consist of Egesen Stadial moraine sequences in two adjacent glacier valleys (Alp Flix 1 and Alp Flix 2), as well as the Egesen moraines of the Lagrev Glacier in Julier Pass, Switzerland (Figure 14).

$\Delta$ ELA reconstructions for Lagrev are based on results from the ELA model for both the Younger Dryas and modern glacier extents. As both Alp Flix 1 and Alp Flix 2 lack modern glaciers, we compare the modeled YD ELA in these valleys to the regional modern proxy ELA obtained from late August snowline measurements (2006-2011) using the supervised classification scheme. The estimated ELAs for these Alp Flix glaciers are comparable to the Lagrev ELAs.

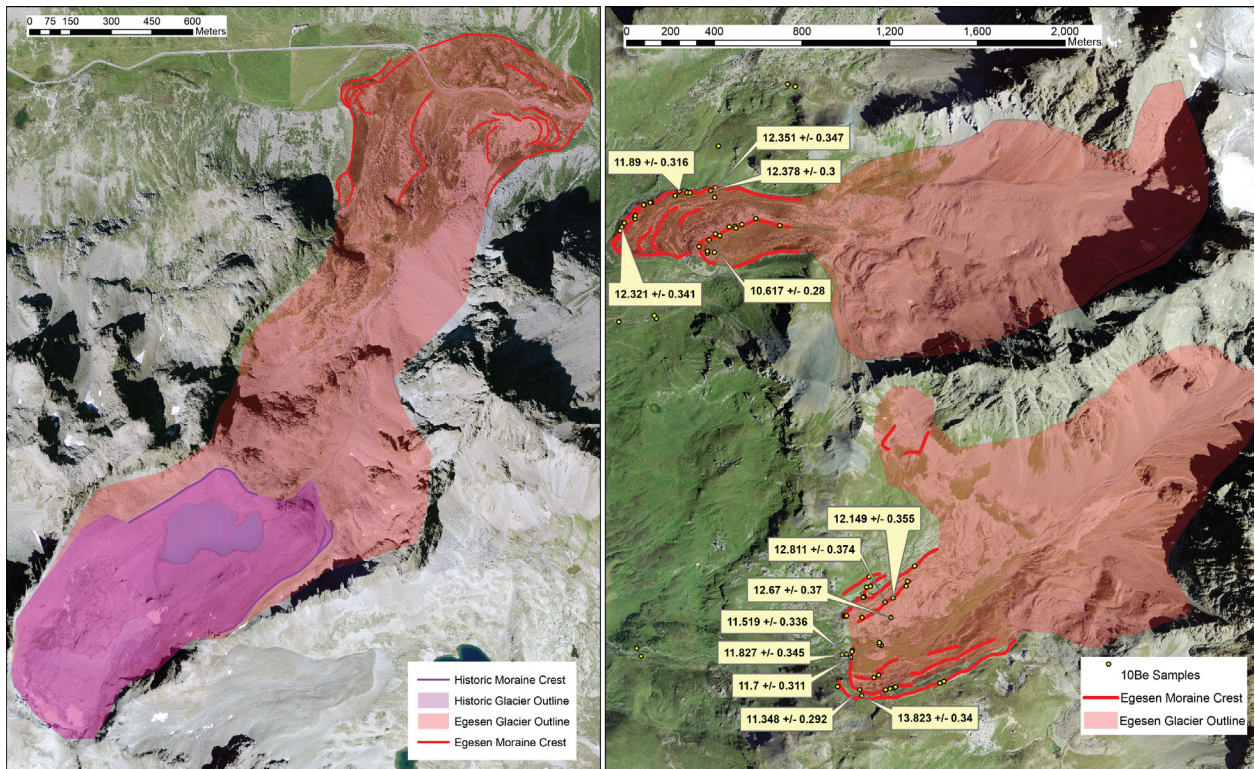


Figure 14. Aerial photographs for the three glacial valleys used in this study. The left shows the Lagrev Glacier in Julier Pass. The right shows the two Alp Flix glacier valleys, Alp Flix 1 (to the south) and Alp Flix 2 (to the north). The Alp Flix glaciers additionally show the location of  $^{10}\text{Be}$  sampling sites, along with the calculated ages. Ivy-Ochs et. al. (1996) has similar age delineations for the Lagrev valley. Red shading represents the proposed Younger Dryas glacier extent, while the purple shading in the Lagrev image shows proposed Little Ice Age glacier extent. Imagery obtained through Swisstopo SWISSIMAGE orthophotomosaic images (resolution  $\pm 2.5$  m).

#### 4.2.1 Age constraints

Figure 14 shows the locations for the moraine boulder samples, along with the  $^{10}\text{Be}$  ages, in the two Alp Flix Valleys and delineations of the target moraines. The Lagrev moraines are similarly delineated in Figure 14. Previous surface exposure dating (Ivy-Ochs et. al., 1996; Ivy-Ochs et al., 2009) correlates the innermost Egesen moraine sequence at Julier Pass (second phase of Egesen Stadial) with the final stages of the Younger Dryas, with a median age of  $11,300 \pm 900$  years before present (BP). New surface exposure ages using  $^{10}\text{Be}$  (presented herein) also correlate the Egesen moraine sequences of the two Alp Flix valleys with the Younger Dryas, with median ages of  $11,988 \pm 234$  years and  $12,351 \pm 189$  years (Figure 15). These results suggest an offset between the stabilization time for the Alp Flix 2 and Lagrev moraines. This could indicate Alp Flix 2 moraines may be associated with the first phase of the Egesen Stadial (earlier *during the Younger Dryas*), or it may indicate a local variation in the factors leading to a difference in the magnitude of change between the two Alp Flix glaciers.

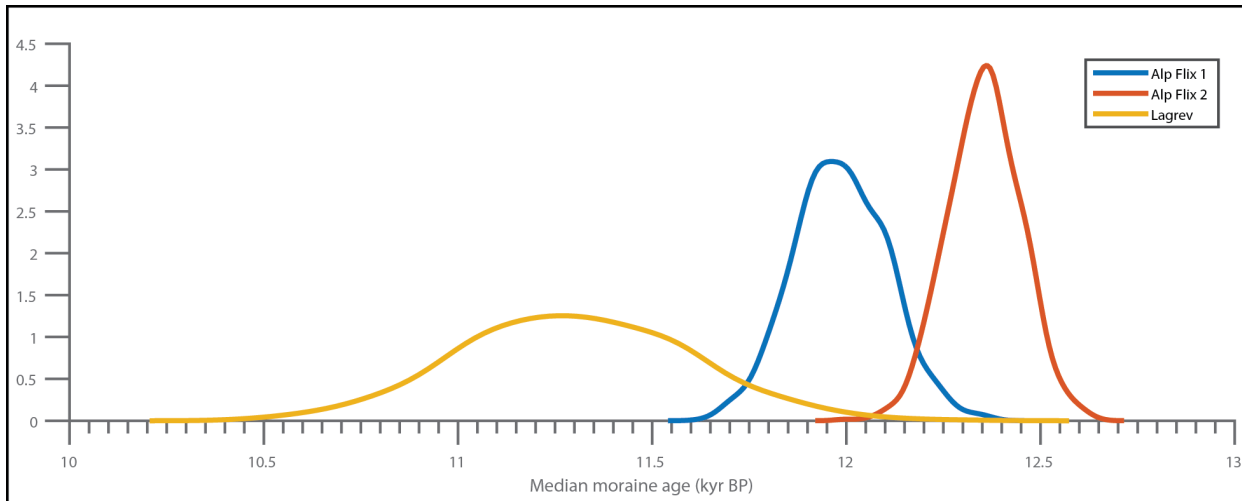


Figure 15. Probability density functions for  $^{10}\text{Be}$  ages of moraines in Alp Flix 1, Alp Flix 2, and Lagrev. Lagrev ages are taken from Ivy Ochs, et. al. (1996). Although all three moraines stabilized during the Younger Dryas, it appears they may differ slightly in age, with Alp Flix 2 as the oldest sequence and Lagrev as the youngest sequence.

#### *4.2.2 ELA Model outputs*

Figures 16-19 summarize the model performance for the bed profile, glacier width, and ice thickness of the two Younger Dryas Alp Flix glaciers and the Lagrev glacier (both Younger Dryas and modern). Elevation data for these valleys are SwissTopo swissALTI3D DEMs, with average resolution of  $\pm 3$  m. SwissTopo SWISSIMAGE orthophotomosaic images (resolution  $\pm 2.5$  m) were used to draw paleoglacier outlines. The model appears to accurately capture all the input parameters, with a few notable outliers, particularly in the modeled glacier widths. As previously stated, the accumulation zones of paleoglaciers are notoriously difficult to delineate precisely. These outliers, therefore, are equally likely to be either the result of model error or incorrect input values. Even with these discrepancies, the model appears well suited to estimate the ELAs of these paleoglaciers.

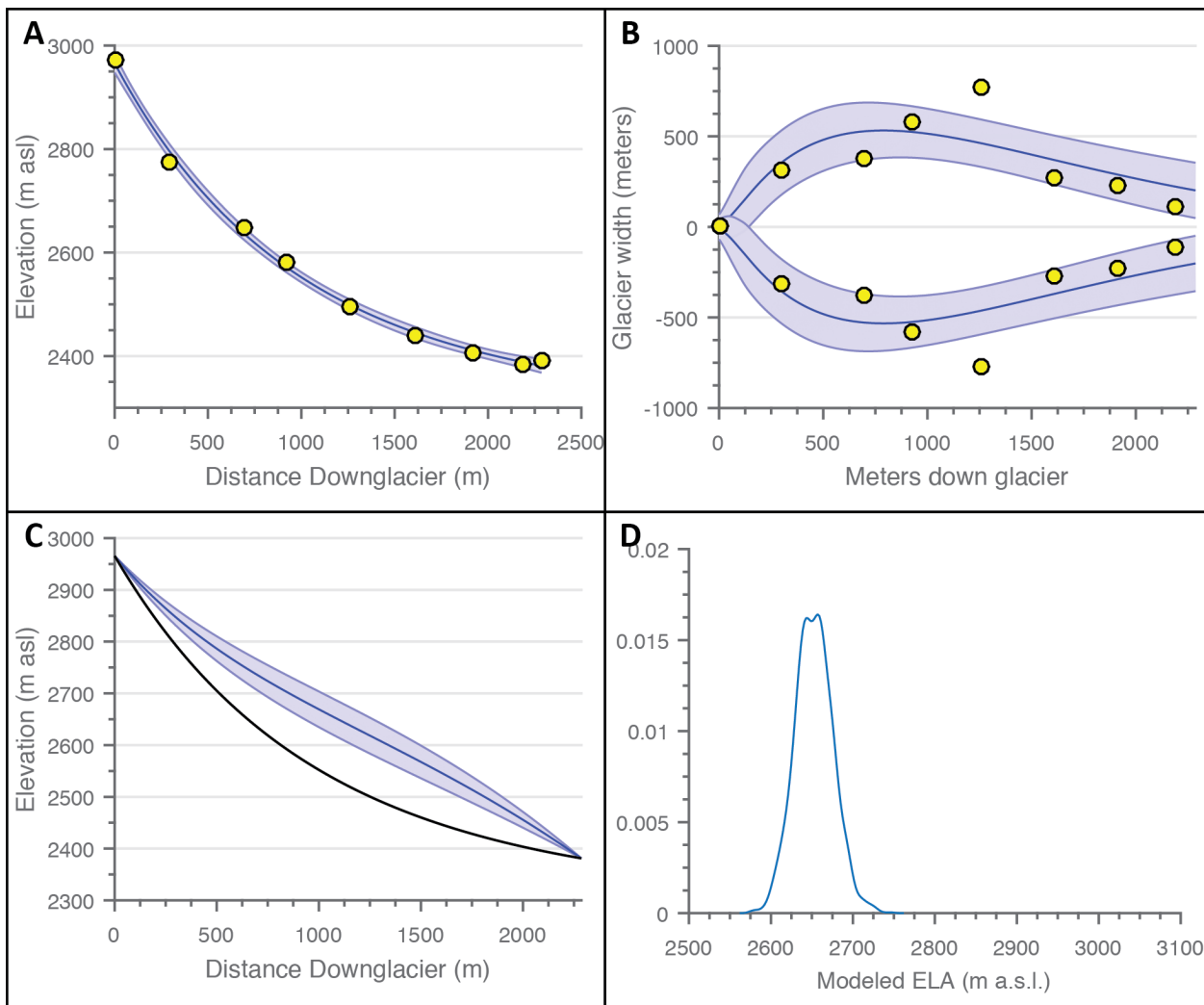


Figure 16. Model outputs for Younger Dryas glacier Alp Flix 1. Panels are as follows: A) glacier bed profile, B) glacier width, C) ice surface profile, and D) probability density curve for modeled ELA values. Yellow circles represent measured input values, solid blue lines (A-C) represent mean model values, and blue shading (A-C) represents model error ( $\pm 2$  standard deviations). The solid black line in C shows the mean modeled bed profile from A. Modeled ELA for this Younger Dryas moraine sequence is  $2652 \text{ m} \pm 46 \text{ m}$ .

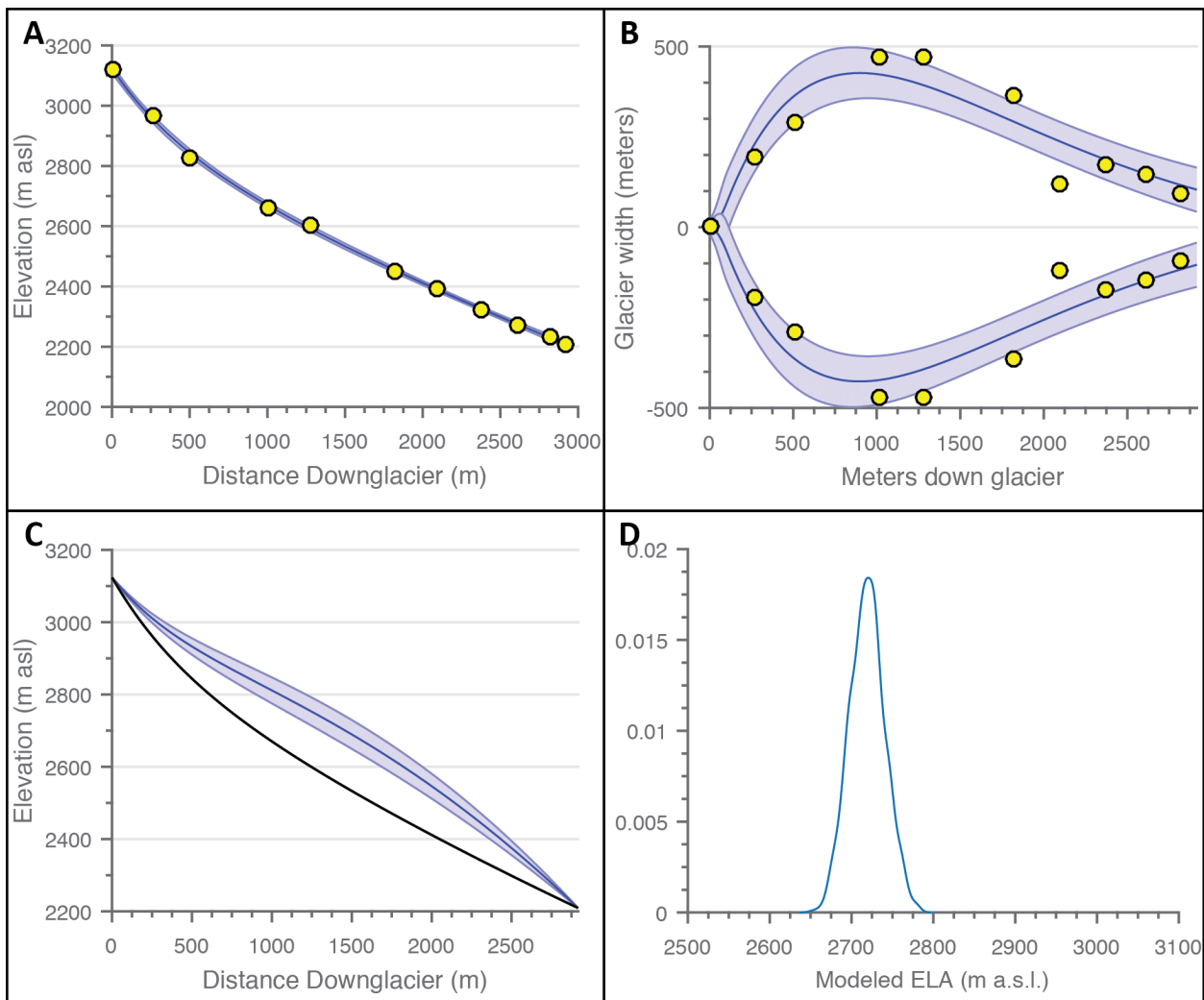
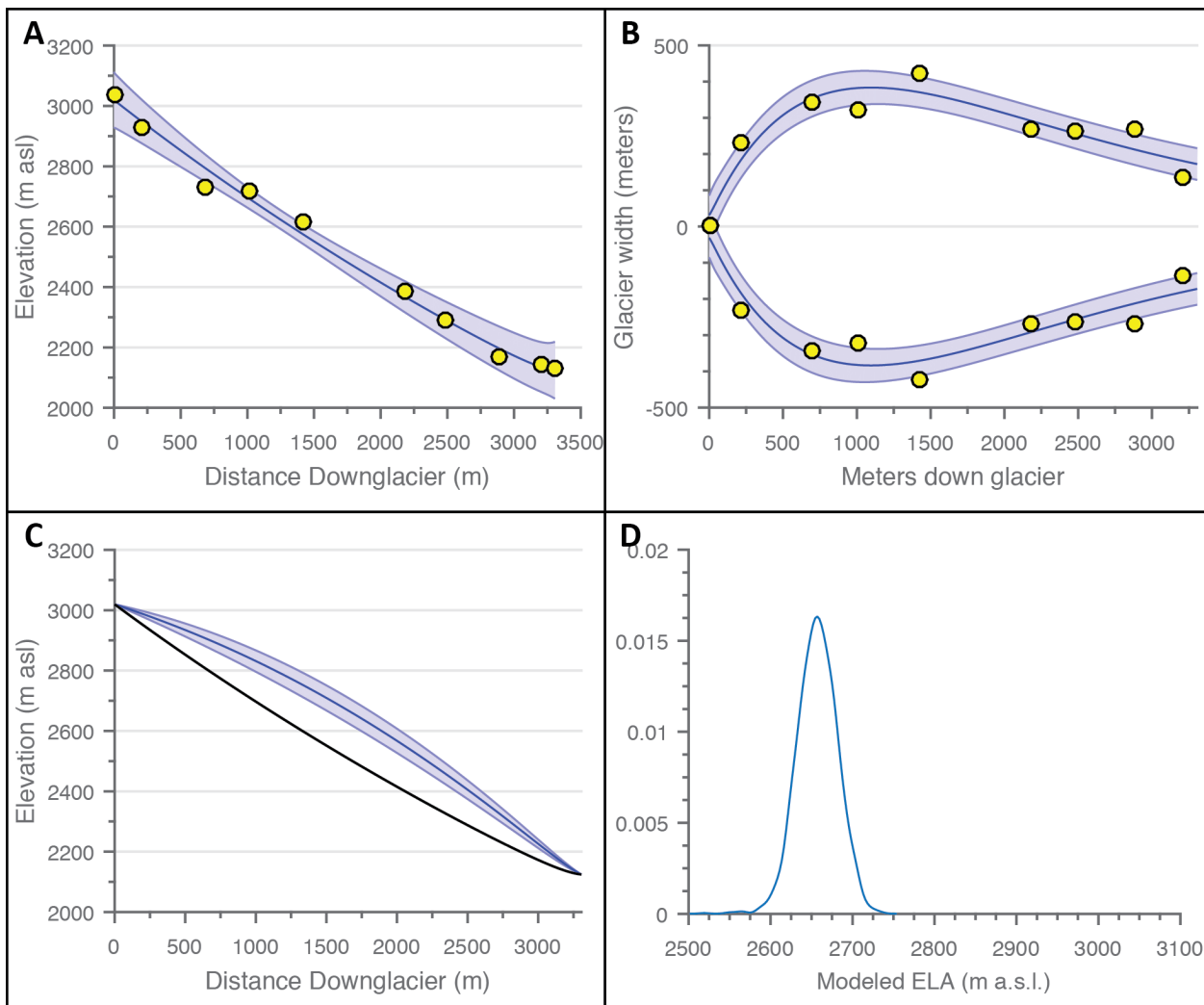
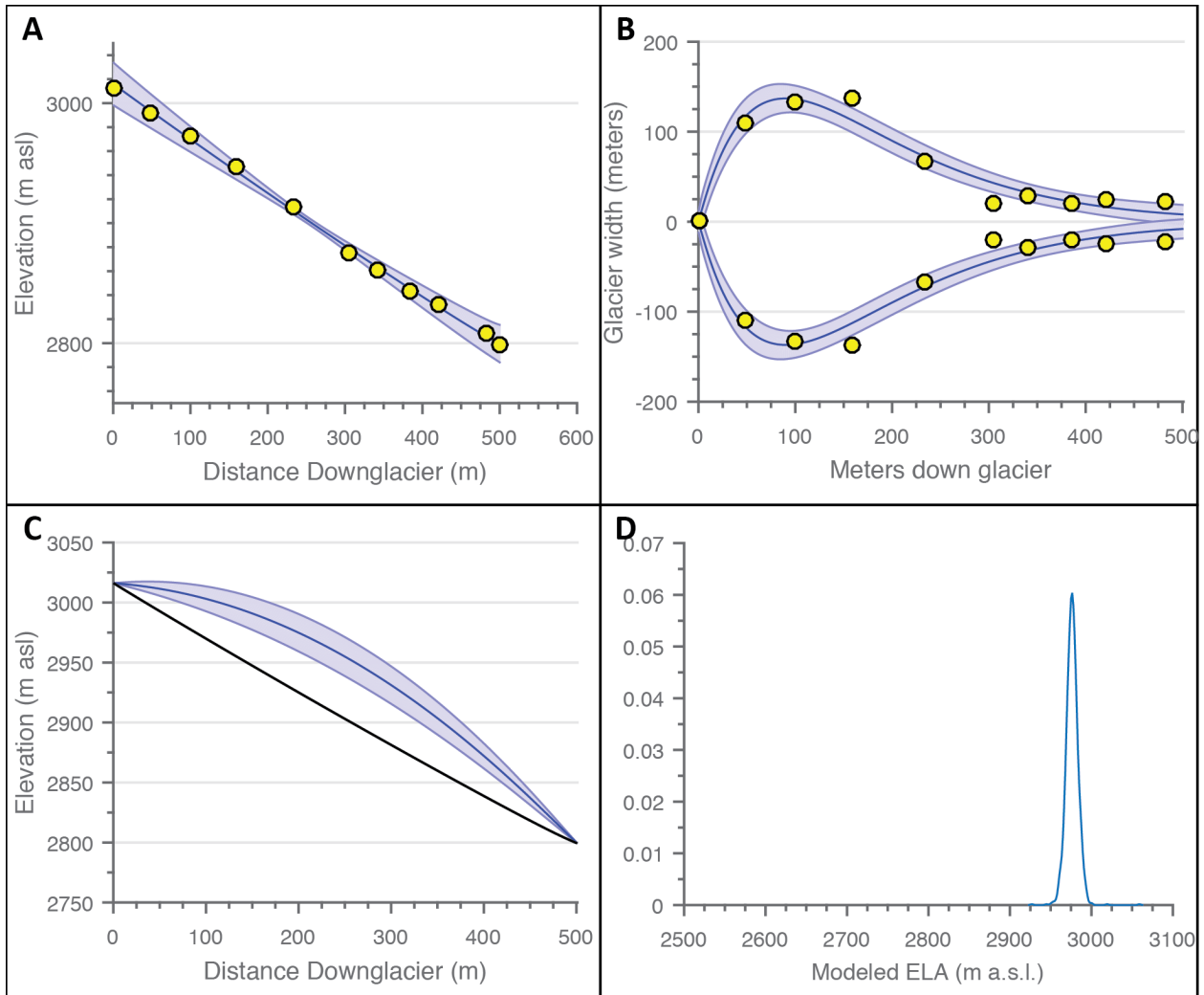


Figure 17. Model outputs for Younger Dryas glacier Alp Flix 2. Panels are as follows: A) glacier bed profile, B) glacier width, C) ice surface profile, and D) probability density curve for modeled ELA values. Yellow circles represent measured input values, solid blue lines (A-C) represent mean model values, and blue shading (A-C) represents model error ( $\pm 2$  standard deviations). The solid black line in C shows the mean modeled bed profile from A. Modeled ELA for this Younger Dryas moraine sequence is  $2719 \text{ m} \pm 44 \text{ m}$ .



*Figure 18. Model outputs for the Younger Dryas glacier in Julier Pass (Lagrev Glacier). Panels are as follows: A) glacier bed profile, B) glacier width, C) ice surface profile, and D) probability density curve for modeled ELA values. Yellow circles represent measured input values, solid blue lines (A-C) represent mean model values, and blue shading (A-C) represents model error ( $\pm 2$  standard deviations). The solid black line in C shows the mean modeled bed profile from A. Modeled ELA for this Younger Dryas moraine sequence is  $2657 \text{ m} \pm 49 \text{ m}$ .*



*Figure 19. Model outputs for the modern glacier in Julier Pass (Lagrev Glacier Panels are as follows: A) glacier bed profile, B) glacier width, C) ice surface profile, and D) probability density curve for modeled ELA values. Yellow circles represent measured input values, solid blue lines (A-C) represent mean model values, and blue shading (A-C) represents model error ( $\pm 2$  standard deviations). The solid black line in C shows the mean modeled bed profile from A. Modeled ELA for this modern glacier boundary is 2976 m  $\pm 15$  m.*

#### 4.2.3 ELA and $\Delta$ ELA comparisons

Figure 20 compares the Younger Dryas absolute ELA and  $\Delta$ ELA results for the Alp Flix 1, Alp Flix 2, and Lagrev paleoglaciers, with the results also summarized in Table 3. Figure 20A shows reasonable agreement between all three absolute ELA values, with a mean ELA of 2676 m for the three glaciers. There is also considerable overlap between the modeled modern ELA at

Lagrev and the proxy ELA results from snowline analysis, supporting the use of the snowline estimate at Alp Flix 1 and Alp Flix 2. The  $\Delta$  ELA results in Figure 20B (the more robust of the two measurements) also show agreement between all three glaciers, particularly between the Lagrev site and Alp Flix 2. There is an offset between these results and the Alp Flix 1, but the difference is not statistically significant at the 95% confidence interval. Similar to the age discrepancy for these moraines (Figure 15), no compelling reason is explicitly evident for this offset, as the similarities in space, time, and orientation argue for similar climate responses between Alp Flix 1 and Alp Flix 2.

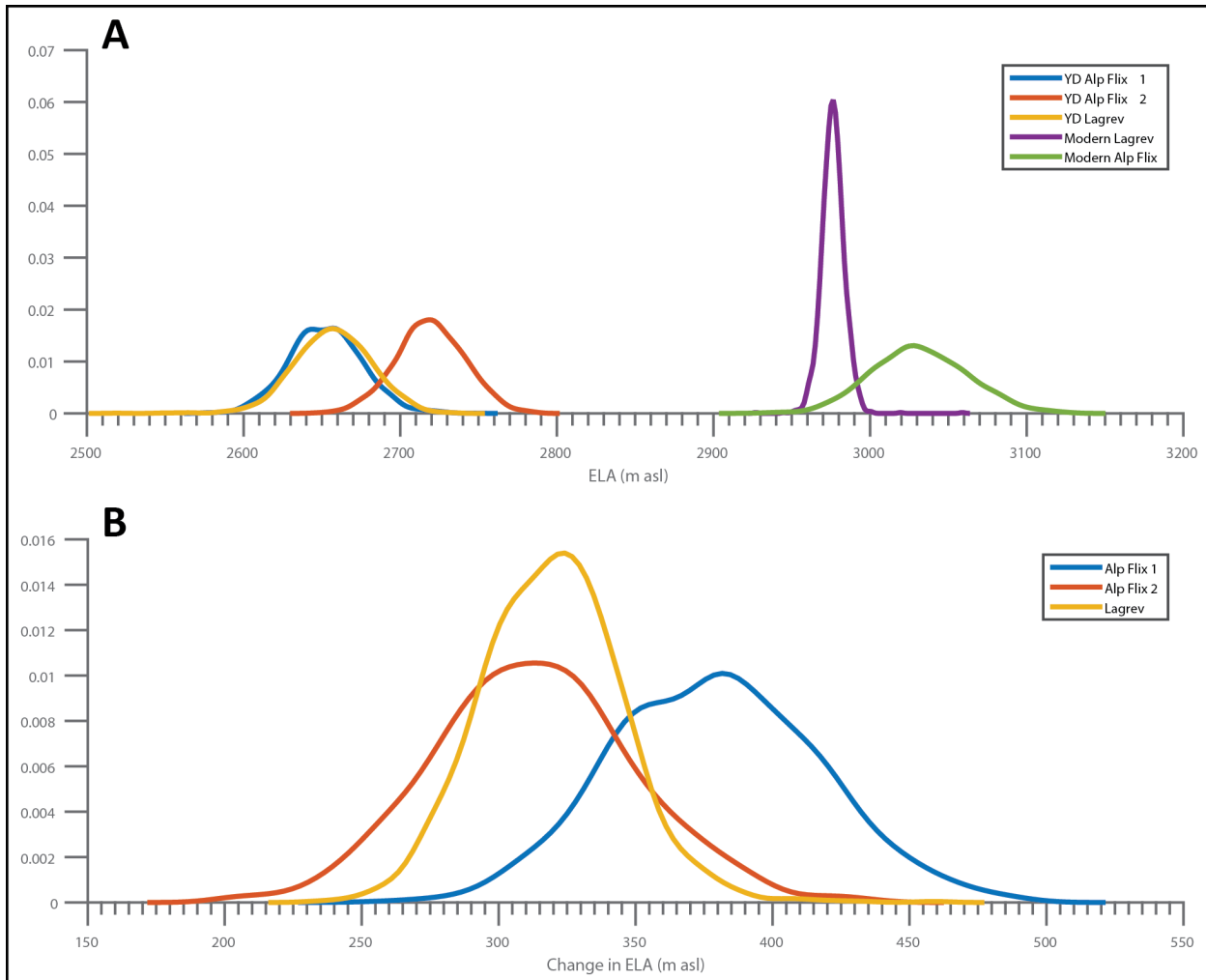


Figure 20. Probability density functions for Younger Dryas absolute ELAs (A) and  $\Delta$  ELAs between the Younger Dryas and present day (B) for Alp Flix 1, Alp Flix 2, and Lagrev glaciers. Note that A also includes the modeled present day ELAs for Lagrev glacier (derived from the model) and for Alp Flix (from the snowline estimate). The mean value for the Younger Dryas ELA in the region (defined from all three glaciers) is 2676 m, compared to the modern ELA of 2976 m. In B,  $\Delta$  ELA functions for the Alp Flix glaciers were calculated from Younger Dryas model results and modern ELA proxies from snowline altitude estimates. Note the overlap in B, indicating that, within errors, all three valleys experienced the same change in ELA.

*Table 3. Summary of ages and ELAs for Lagrev, Alp Flix 1, and Alp Flix 2 glaciers*

Glacier system	Median Age (ka)	Error	YD ELA (m a.s.l.)	Error	Modern ELA (m a.s.l.)	Error	ΔELA	Error
Alp Flix 1 (YD-modern)	11.988	±0.234	2,652	±46	3,033*	±61	381 m	±75
Alp Flix 2 (YD-modern)	12.351	±0.189	2,719	±44	3,033*	±61	314 m	±73
Lagrev (YD-modern)	11.300	±0.600	2,657	±49	2,976	±15	320 m	±51

\*Denotes ELA estimate from snowline classification

#### 4.2.4 Temperature and precipitation reconstructions

As mentioned previously, one of the shortcomings of ELA models, or any glacier-change estimate, is an inability to differentiate between the different potential causes of a change in climate. In the simplest case, glaciers respond to changes in both temperature and precipitation. A change in ELA can be a result of changes in any combination of these two factors. Investigations of changes to temperature and precipitation based on ELA reconstructions, however, can still be useful for a variety of reasons. Such studies still allow for investigations of relative climate sensitivities to temperature vs. precipitation. Additionally, if previous independent results provide constraints on one of these variables (e.g., precipitation changes from paleo-lake records), the measured change in ELA can be used to estimate the other variable.

Using the PDD model detailed in the Methodology, we reconstruct the full range of likely precipitation and temperature changes required to account for the ELA change between the YD and modern day climate observed in the Lagrev system (Figure 21). We focus on the Lagrev

reconstructions for consistency of reconstruction techniques and due to the higher certainty in the  $\Delta$  ELA for that system, even though both Alp Flix 1 and Alp Flix 2 offer similar  $\Delta$  ELAs. As seen in Figure 21, if winter precipitation did not change (e.g., same as present-day mean snowfall), mean annual temperature would be  $2.18^{\circ}\text{C} \pm 1.33^{\circ}\text{C}$  cooler relative to today to produce the Younger Dryas glacier extent observed at Lagrev. Assuming no change in temperature at the Younger Dryas relative to present-day, winter precipitation would need to be 291%  $\pm$  86% greater than today. Some studies, however, suggest precipitation decreased during the YD, which would increase the temperature cooling required to explain the ELA changes. Accounting for a decrease in precipitation of 30% (e.g., Kerschner et. al., 2000; Heiri et. al. 2014) increases the change in annual temperature slightly to  $\Delta T = -2.29^{\circ}\text{C} \pm 1.32^{\circ}\text{C}$ .

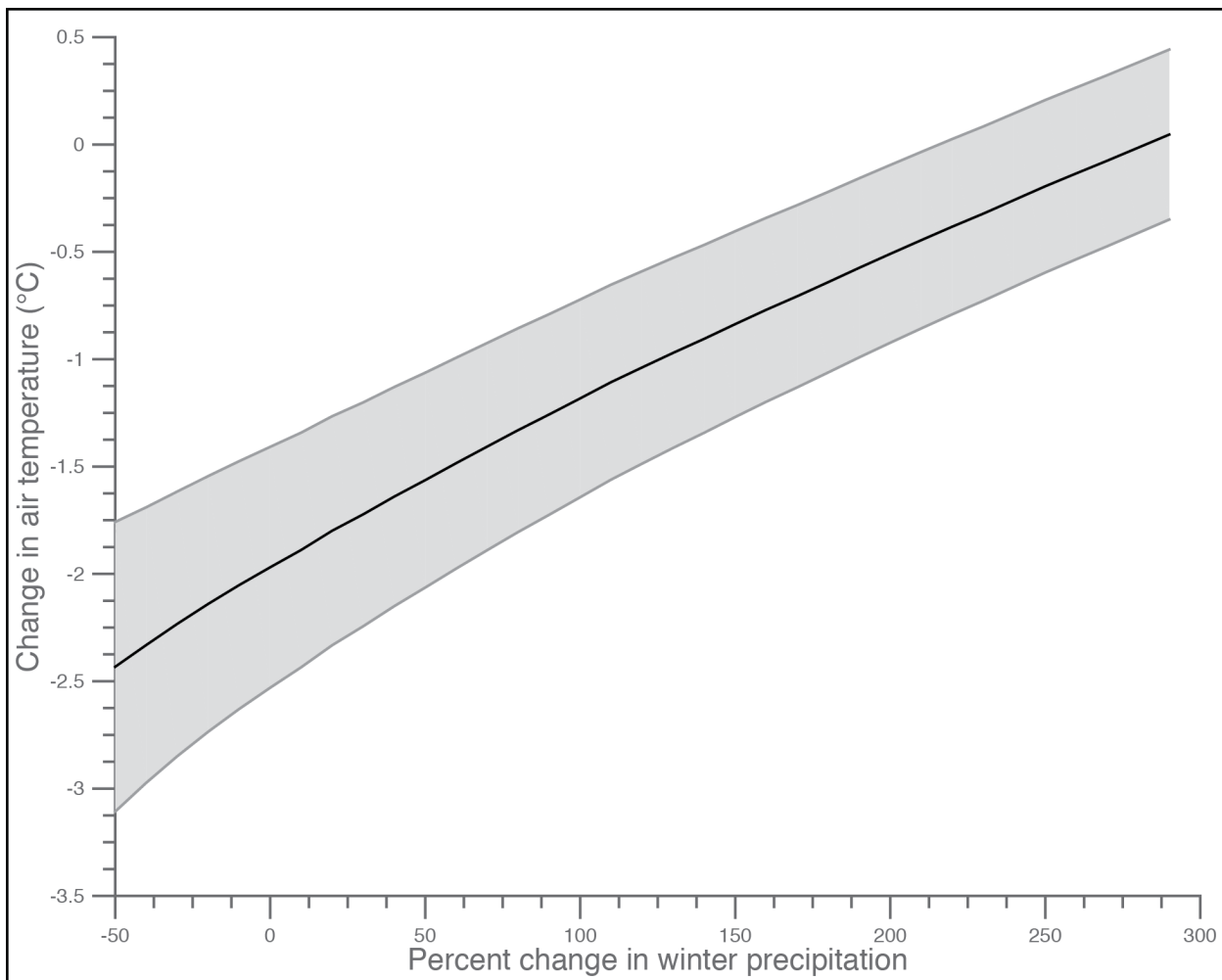


*Figure 21. Modeled range in changes in temperature and precipitation between the Younger Dryas and present day for the Lagrev Glacier. The black line denotes the spectrum of  $\Delta T$ - $\Delta P$  combinations that could produce the estimated  $\Delta$ ELA, with grey shading representing the  $\pm 2$  standard deviation uncertainty on those results. Assuming a 30% decrease in precipitation, annual temperatures during the Younger Dryas were  $2.29^{\circ}\text{C} \pm 1.32^{\circ}\text{C}$  cooler than today.*

## 5 DISCUSSION

ELAs in the Swiss Alps, specifically in the Julier Pass and Alp Flix regions, lowered by 320  $\pm 51$  m during the YD relative to the present day. Comparisons of this ELA depression to previous work is complicated by the fact that most previous studies report European ELA depressions relative to the Little Ice Age (LIA) extent. Although not currently analytically constrained, the Lagrev valley appears to have a well-preserved moraine sequence from the LIA

(Figure 14). The lack of vegetation and overall fresh appearance lend credence to this assumption, with previous studies assuming likewise (e.g. Ivy-Ochs et. al., 2007). Using this historic moraine sequence and the moraine sets previously constrained to the late YD by Ivy-Ochs et. al. (1996), we estimate the  $\Delta$  ELA between the YD and LIA at this site as  $213 \text{ m} \pm 54 \text{ m}$ . Heiri et al (2014) gives typical values for the YD ELA depression of 200-250 m relative to LIA for the central Alps. These results are reaffirmed by numerous other studies on glacier valleys in the Alps (Ivy-Ochs et al, 2009; Ivy-Ochs et al, 2006; Hormes et al, 2008; Burga, 1987; Suter, 1981; and others), although some studies suggest higher  $\Delta$  ELA values for at least some regions of the Alps (e.g. Kerschner et. al., 2000; Federici et. al., 2008). The  $\Delta$  ELA results of this study therefore agree well with many previous estimates in the area, but offer additional explicit constraints on the uncertainty of the results, and a means by which to compare directly to present-day climate (unlike the LIA approach).

Such consistency throughout different studies and locations in the area indicates that ELA change during the Younger Dryas was broadly uniform across the central Alps. It is currently unclear how much of the variation that does exist between different sites results from local climate/glacier variability or from differences in ELA reconstruction methods. Future studies with the proposed ELA model will investigate the local and regional variability in the Younger Dryas climate response in the Alps, allowing for direct comparisons between sites.

The climate reconstructions in this study suggest a strong dependence on temperature for YD glaciers in the Graubünden Alps, with less sensitivity to changes in precipitation. This fits expectations for alpine temperate glaciers, where much of the ablation during the year occurs due to melt in the summertime (Rupper et al., 2008; Ivy-Ochs et. al., 2009; Heiri et. al., 2014). Our

results show that even relatively small changes in temperature of  $\sim 2$  °C will dominate even large changes in winter precipitation.

Significant effort has focused on temperature reconstructions in the Alps from other paleoclimate proxy methods. These reconstructions range from a 1 °C to nearly 7 °C decrease in summer temperature (based on pollen, speleothem, glacier, chironomid, and timberline records) (Table 4). In an effort to make our results more directly comparable to studies reconstructing summer temperature, we include the estimated change in mean summer temperature (here defined as the ablation season) from our PDD model for ease of comparison.

*Table 4. Summary of Younger Dryas temperature reconstructions (various methodologies)*

Location	Reconstruction type	Proxy used	$\Delta T$ (°C)	Error	Source
Northern Alps foreland	Summer temperature	Pollen and cladocera	6.9	$\pm 1.50$	Lotter et. al., 2000
Southern Alps foreland	July air temperature	Chironomids	6.0	$\pm 1.60$	Samartin et. al., 2012a
South central Alps	July air temperature	Chironomids	2.4	$\pm 1.50$	Samartin et. al., 2012b
South central Alps	July air temperature	Chironomids	2.0	$\pm 1.36$	Illyashuk et. al., 2009
South central Alps	Annual temperature	ELA/PDD model	2.29	$\pm 1.32$	This study
South central Alps	Summer temperature	ELA/PDD model	1.47	$\pm 0.73$	This study
Swiss Alps (general)	Annual temperature	Rock glacier elevation	3.5+	*NA	Ivy-Ochs et. al., 2009
Swiss Alps (general)	Summer temperature	Timberline depression	3.5	*NA	Kerschner et. al., 2000

\*Not available

Our work places temperature changes towards the lower end of these estimates, and suggests, within the uncertainties, fairly small changes in temperature can give rise to large changes in glaciers in this region. Furthermore, our results indicate small changes specifically in summer temperatures are sufficient to drive the observed changes in glacier extent during the

Younger Dryas cold phase. To explain these small changes in summer temperature relative to the larger changes in annual air temperature, the mechanisms proposed to drive the YD cold reversal must explain the relatively small changes in summer temperature. For example, changes in seasonality (e.g., larger changes in winter relative to summer) or significant increases in snowfall (counter to most paleoclimate proxy data) are possible explanations.

A distinct advantage of these ELA based reconstructions over other methods of paleoclimate reconstruction is their simplicity and ease of use. While many of these other paleoclimate methods require fieldwork, in-situ sample collection, and lengthy laboratory analysis, this ELA model can be readily applied using publicly available remote sensing data. Obtaining final results for individual glaciers (data collection, calculations, and uncertainty characterization) is possible in a single day, at virtually no cost to the researcher. Although this requires careful selection of study sites previously temporally constrained, such glacial chronologies are ever-increasingly available. These low requirements of time and resources make this approach a compelling choice for many paleoclimate investigations.

## 6 CONCLUSIONS

A new ELA model that accounts for glacier hypsometry and does not make direct assumptions about the climate system offers a physically based alternative to empirical paleo-ELA reconstruction methods, while also providing objective uncertainty estimates using Monte Carlo simulations. The model is tested for accuracy in reproducing glacier bed profiles, glacier plan boundaries, ice thickness, and ELAs with validation against four separate glaciers in the Swiss Alps. The model is shown to capture present-day ELAs within the uncertainties of the model and the measurements. This model should therefore serve as a robust, easily applicable,

self-consistent method for ELA reconstructions in diverse areas. Application of this model to three glacier valleys in the Graubünden Alps yields a Younger Dryas ELA depression of -320 m  $\pm$ 51 m relative to present day (-216 m  $\pm$  52 m relative to LIA extent). Such results compare favorably with previous studies in the area for the Younger Dryas, but provide the added ability to assess whether ELA changes are statistically significant over space and time.

A simple temperature index model translates the  $\Delta$  ELA calculated for the Younger Dryas to a change in mean annual temperature relative to today of  $\Delta T = -2.29^{\circ}\text{C} \pm 1.32^{\circ}\text{C}$ . Summer temperatures only  $1.47^{\circ}\text{C} \pm 0.73^{\circ}\text{C}$  cooler than today are sufficient to reproduce the Younger Dryas extent of the tested glaciers in the south central Alps. Our results suggest Younger Dryas temperature changes were on the low end of previous estimates in the region from fossil pollen, chironomid assemblages, and previous glacial studies. In addition, these results suggest Younger Dryas glaciers were likely more sensitive to air temperature, especially summer temperatures, than to winter precipitation changes.

Such results add to the growing evidence that small changes in temperature can produce drastic changes in glaciers. Such conclusions obviously have important implications not only for paleoclimate studies, but also for future warming. Glaciers and glacier melt are important components of water resources in many areas around the globe, including uses for drinking, irrigation, and power generation. The forecasted changes in air temperature in the near future will likely have a massive effect on the overall water budget in these glacierized regions, with far-reaching effects on the surrounding populations. Continued research into abrupt changes in climate both in the past and present, and the effect such changes exhibit on glaciers, will help elucidate the mechanisms of these abrupt changes. This will in turn help us better understand and prepare for future climate impacts on nations and society at large.

## 7 REFERENCES

Alley, R. B. and A. M. Ágústsdóttir (2005), The 8k event: cause and consequences of a major

Holocene abrupt climate change, *Quaternary Science Reviews*, 24(10), 1123-1149.

Alley, R. B., J. Marotzke, W. D. Nordhaus, J. T. Overpeck, D. M. Peteet, R. A. Pielke Jr, R. T.

Pierrehumbert, P. B. Rhines, T. F. Stocker, L. D. Talley, and J. M. Wallace (2003), Abrupt climate change, *Science*, 299(5615), 2005-2010, doi:10.1126/science.1081056 [doi].

Benn, D. I. and F. Lehmkuhl (2000), Mass balance and equilibrium-line altitudes of glaciers in high-mountain environments, *Quaternary International*, 65, 15-29.

Braithwaite, R. J. (1995), Positive degree-day factors for ablation on the Greenland ice sheet studied by energy-balance modelling, *J. Glaciol.*, 41(137), 153-160.

Braithwaite, R. J. and Y. Zhang (2000), Sensitivity of mass balance of five Swiss glaciers to temperature changes assessed by tuning a degree-day model, *J. Glaciol.*, 46(152), 7-14.

Briner, J. P. (2011), Dating Glacial Landforms, in *Encyclopedia of Snow, Ice and Glaciers*, , edited by Anonymous , pp. 175-176, Springer.

Broecker, W. S. (1997), Thermohaline circulation, the achilles heel of our climate system: will man-made CO<sub>2</sub> upset the current balance? *Science*, 278(5343), 1582-1588.

Bronge<sup>†</sup>, L. B. and C. Bronge<sup>†\*</sup> (1999), Ice and snow-type classification in the Vestfold Hills, East Antarctica, using Landsat-TM data and ground radiometer measurements, Int. J. Remote Sens., 20(2), 225-240.

Burga, C. A. (1987), Gletscher-und Vegetationsgeschichte der südrätischen Alpen seit der Späteiszeit:(Puschlav, Livigno, Bormiese), vol. 101, , Birkhauser, .

Carlson, A. (2013), The younger dryas climate event, in The Encyclopedia of Quaternary Science, , vol. 3, edited by Anonymous , pp. 126-134, Elsevier Amsterdam.

Colgan, W., W. Pfeffer, H. Rajaram, W. Abdalati, and J. Balog (2012), Monte Carlo ice flow modeling projects a new stable configuration for Columbia Glacier, Alaska, c. 2020, The Cryosphere, 6(6), 1395-1409.

Cox, L. H. and R. S. March (2004), Comparison of geodetic and glaciological mass-balance techniques, Gulkana Glacier, Alaska, USA, J. Glaciol., 50(170), 363-370.

Cuffey, K. M. and W. S. B. Paterson (2010), The physics of glaciers, Academic Press, .

Doughty, A. M., B. M. Anderson, A. N. Mackintosh, M. R. Kaplan, M. J. Vandergoes, D. J. Barrell, G. H. Denton, J. M. Schaefer, T. J. Chinn, and A. E. Putnam (2013), Evaluation of Lateglacial temperatures in the Southern Alps of New Zealand based on glacier modelling at Irishman Stream, Ben Ohau Range, Quaternary Science Reviews, 74, 160-169.

Farinotti, D. (2010) Simple methods for inferring glacier ice-thickness and snow-accumulation distribution.

Farinotti, D., M. Huss, A. Bauder, M. Funk, and M. Truffer (2009), A method to estimate the ice volume and ice-thickness distribution of alpine glaciers, *J. Glaciol.*, 55(191), 422-430.

Furbish, D. and J. Andrews (1984), The use of hypsometry to indicate long-term stability and response of valley glaciers to changes in mass transfer, *J. Glaciol.*, 30(105), 199-211.

Goehring, B. M., D. A. Vacco, R. B. Alley, and J. M. Schaefer (2012), Holocene dynamics of the Rhone Glacier, Switzerland, deduced from ice flow models and cosmogenic nuclides, *Earth Planet. Sci. Lett.*, 351, 27-35.

Gosse, J. C., E. Evenson, J. Klein, B. Lawn, and R. Middleton (1995), Precise cosmogenic  $^{10}\text{Be}$  measurements in western North America: Support for a global Younger Dryas cooling event, *Geology*, 23(10), 877-880.

Gosse, J. C., E. Evenson, J. Klein, B. Lawn, and R. Middleton (1995), Precise cosmogenic  $^{10}\text{Be}$  measurements in western North America: Support for a global Younger Dryas cooling event, *Geology*, 23(10), 877-880.

Gosse, J. C. and F. M. Phillips (2001), Terrestrial *in situ* cosmogenic nuclides: theory and application, *Quaternary Science Reviews*, 20(14), 1475-1560.

Haeberli, W. and M. Hözle (1995), Application of inventory data for estimating characteristics of and regional climate-change effects on mountain glaciers: a pilot study with the European Alps, *Annals of glaciology*, 21, 206-212.

Heiri, O., K. A. Koinig, C. Spötl, S. Barrett, A. Brauer, R. Drescher-Schneider, D. Gaar, S. Ivy-Ochs, H. Kerschner, and M. Luetscher (2014), Palaeoclimate records 60–8 ka in the Austrian and Swiss Alps and their forelands, *Quaternary Science Reviews*, 106, 186-205.

Hock, R. (2003), Temperature index melt modelling in mountain areas, *Journal of Hydrology*, 282(1), 104-115.

Hock, R. (2005), Glacier melt: a review of processes and their modelling, *Prog. Phys. Geogr.*, 29(3), 362-391.

Hormes, A., S. Ivy-Ochs, P. W. Kubik, L. Ferreli, and A. M. Michetti (2008), <sup>10</sup>Be exposure ages of a rock avalanche and a late glacial moraine in Alta Valtellina, Italian Alps, *Quaternary International*, 190(1), 136-145.

Ilyashuk, B., E. Gobet, O. Heiri, A. F. Lotter, J. F. van Leeuwen, van der Knaap, Willem O, E. Ilyashuk, F. Oberli, and B. Ammann (2009), Lateglacial environmental and climatic changes at the Maloja Pass, Central Swiss Alps, as recorded by chironomids and pollen, *Quaternary Science Reviews*, 28(13), 1340-1353.

IPCC (2001), Contribution of working group I to the Third Assessment Report of the Intergovernmental Panel on Climate Change, in Climate change 2001: the scientific basis, pp. 881, Cambridge, UK, Cambridge University Press.

Ivy-Ochs, S., H. Kerschner, P. W. Kubik, and C. Schlüchter (2006), Glacier response in the European Alps to Heinrich Event 1 cooling: the Gschnitz stadial, *Journal of Quaternary Science*, 21(2), 115-130.

Ivy-Ochs, S., H. Kerschner, M. Maisch, M. Christl, P. W. Kubik, and C. Schlüchter (2009), Latest Pleistocene and Holocene glacier variations in the European Alps, *Quaternary Science Reviews*, 28(21), 2137-2149.

Ivy-Ochs, S., H. Kerschner, and C. Schlüchter (2007), Cosmogenic nuclides and the dating of Lateglacial and Early Holocene glacier variations: the Alpine perspective, *Quaternary International*, 164, 53-63.

Ivy-Ochs, S., C. Schlüchter, P. W. Kubik, H. Synal, J. Beer, and H. Kerschner (1996), The exposure age of an Egesen moraine at Julier Pass, Switzerland, measured with the cosmogenic radionuclides  $^{10}\text{Be}$ ,  $^{26}\text{Al}$  and  $^{36}\text{Cl}$ , *Eclogae Geologicae Helvetiae*, 89(3), 1049-1064.

Kaplan, M. R., J. M. Schaefer, G. H. Denton, D. J. Barrell, T. J. Chinn, A. E. Putnam, B. G. Andersen, R. C. Finkel, R. Schwartz, and A. M. Doughty (2010), Glacier retreat in New Zealand during the Younger Dryas stadial, *Nature*, 467(7312), 194-197.

Kaplan, M. R., J. M. Schaefer, G. H. Denton, D. J. Barrell, T. J. Chinn, A. E. Putnam, B. G. Andersen, R. C. Finkel, R. Schwartz, and A. M. Doughty (2010), Glacier retreat in New Zealand during the Younger Dryas stadial, *Nature*, 467(7312), 194-197.

Kerschner, H. (2004), Climate in the central Alps, 16,000 years ago - the case of the Gschnitz Stadial, Geophysical Research Abstracts, 6(EGU04-A-04695).

Kerschner, H. (2005), Glacier-climate models as palaeoclimatic information sources: Examples from the Alpine Younger Dryas period, in Global Change and Mountain Regions, , edited by Anonymous , pp. 73-81, Springer.

Kerschner, H. and S. Ivy-Ochs (2008), Palaeoclimate from glaciers: Examples from the Eastern Alps during the Alpine Lateglacial and early Holocene, Global Planet. Change, 60(1), 58-71.

Kerschner, H., G. Kaser, and R. Sailer (2000), Alpine Younger Dryas glaciers as palaeo-precipitation gauges, Annals of Glaciology, 31(1), 80-84.

Konz, M. and J. Seibert (2010), On the value of glacier mass balances for hydrological model calibration, Journal of hydrology, 385(1), 238-246.

Kroese, D. P., T. Taimre, and Z. I. Botev (2013), Handbook of Monte Carlo Methods, vol. 706, , John Wiley & Sons, .

Kuczera, G. and E. Parent (1998), Monte Carlo assessment of parameter uncertainty in conceptual catchment models: the Metropolis algorithm, Journal of Hydrology, 211(1), 69-85.

Kuhn, M. (1984), Mass budget imbalances as criterion for a climatic classification of glaciers, Geografiska Annaler.Series A.Physical Geography, 229-238.

Leonard, K. C. and A. G. Fountain (2003), Map-based methods for estimating glacier equilibrium-line altitudes, *J. Glaciol.*, 49(166), 329-336.

Lotter, A., H. Birks, U. Eicher, W. Hofmann, J. Schwander, and L. Wick (2000), Younger Dryas and Allerød summer temperatures at Gerzensee (Switzerland) inferred from fossil pollen and cladoceran assemblages, *Palaeogeogr. , Palaeoclimatol. , Palaeoecol.*, 159(3), 349-361.

Machguth, H., R. Purves, J. Oerlemans, M. Hoelzle, and F. Paul (2008), Exploring uncertainty in glacier mass balance modelling with Monte Carlo simulation, *The Cryosphere*, 2(2), 191-204.

Mayewski, P. A., E. E. Rohling, J. C. Stager, W. Karlén, K. A. Maasch, L. D. Meeker, E. A. Meyerson, F. Gasse, S. van Kreveld, and K. Holmgren (2004), Holocene climate variability, *Quatern. Res.*, 62(3), 243-255.

McFadden, E., J. Ramage, and D. Rodbell (2011), Landsat TM and ETM derived snowline altitudes in the Cordillera Huayhuash and Cordillera Raura, Peru, 1986-2005, *The Cryosphere*, 5(2), 419.

Mölg, T., F. Maussion, W. Yang, and D. Scherer (2012), The footprint of Asian monsoon dynamics in the mass and energy balance of a Tibetan glacier, *The Cryosphere*, 6(6), 1445-1461.

Nussbaumer, S. U., F. Steinhilber, M. Trachsel, P. Breitenmoser, J. Beer, A. Blass, M. Grosjean, A. Hafner, H. Holzhauser, and H. Wanner (2011), Alpine climate during the Holocene: a comparison between records of glaciers, lake sediments and solar activity, *Journal of Quaternary Science*, 26(7), 703-713.

Oerlemans, J. (2011), Minimal glacier models,Igitur, Utrecht Publishing & Services,  
Universiteitsbibliotheek Utrecht.

Osmaston, H. (2005), Estimates of glacier equilibrium line altitudes by the Area $\times$  Altitude, the  
Area $\times$  Altitude Balance Ratio and the Area $\times$  Altitude Balance Index methods and their  
validation, Quaternary International, 138, 22-31.

Overpeck, J. T. and J. E. Cole (2006), Abrupt change in Earth's climate system,  
Annu.Rev.Environ.Resour., 31, 1-31.

PSFG (1967): Fluctuations of Glaciers 1959-1965 (Vol. I). P. Kasser (ed.), IAHS (ICSI) / UNESCO,  
Permanent Service on Fluctuations on Glaciers, Zurich, Switzerland: 52 pp.

PSFG (1973): Fluctuations of Glaciers 1965-1970 (Vol. II). P. Kasser (ed.), IAHS (ICSI) / UNESCO,  
Permanent Service on Fluctuations on Glaciers, Zurich, Switzerland: 357 pp.

PSFG (1977): Fluctuations of Glaciers 1970-1975 (Vol. III). F. Müller (ed.), IAHS (ICSI) / UNESCO,  
Permanent Service on Fluctuations on Glaciers, Zurich, Switzerland: 269 pp.

PSFG (1985): Fluctuations of Glaciers 1975-1980 (Vol. IV). W. Haeberli (ed.), IAHS (ICSI) /  
UNESCO, Permanent Service on Fluctuations on Glaciers, Zurich, Switzerland: 265 pp.

Rabatel, A., A. Letréguilly, J. Dedieu, and N. Eckert (2013), Changes in glacier equilibrium-line  
altitude in the western Alps from 1984 to 2010: evaluation by remote sensing and modeling of  
the morpho-topographic and climate controls, Cryosphere, 7(5), p. 1455-p. 1471.

Rupper, S., G. Roe, and A. Gillespie (2009), Spatial patterns of Holocene glacier advance and retreat in Central Asia, *Quatern. Res.*, 72(3), 337-346.

Samartin, S., O. Heiri, A. Lotter, and W. Tinner (2012), Climate warming and vegetation response after Heinrich event 1 (16 700–16 000 cal yr BP) in Europe south of the Alps, *Climate of the Past*, 8(6), 1913-1927.

Samartin, S., O. Heiri, E. Vescovi, S. J. Brooks, and W. Tinner (2012), Lateglacial and early Holocene summer temperatures in the southern Swiss Alps reconstructed using fossil chironomids, *Journal of Quaternary Science*, 27(3), 279-289.

Schaefer, J. M., G. H. Denton, M. Kaplan, A. Putnam, R. C. Finkel, D. J. Barrell, B. G. Andersen, R. Schwartz, A. Mackintosh, T. Chinn, and C. Schluchter (2009), High-frequency Holocene glacier fluctuations in New Zealand differ from the northern signature, *Science*, 324(5927), 622-625, doi:10.1126/science.1169312 [doi].

SPIESS, M., F. MAUSSION, M. MÖLLER, D. SCHERER, and C. SCHNEIDER (2015), MODIS DERIVED EQUILIBRIUM LINE ALTITUDE ESTIMATES FOR PUROGANGRI ICE CAP, TIBETAN PLATEAU, AND THEIR RELATION TO CLIMATIC PREDICTORS (2001–2012), *Geografiska Annaler: Series A, Physical Geography*.

Suter, J. (1981), *Gletschergeschichte des Oberengadins: Untersuchung von Gletscherschwankungen in der Err-Julier-Gruppe*, vol. 464, , Geographisches Institut, Universität Zürich, .

Tarasov, L. (2012), Glacial systems model calibration: Quantifying uncertainty in glaciological reconstructions of past ice-sheets, paper presented at EGU General Assembly Conference

Abstracts.

Tarasov, L., A. S. Dyke, R. M. Neal, and W. Peltier (2012), A data-calibrated distribution of deglacial chronologies for the North American ice complex from glaciological modeling, *Earth Planet. Sci. Lett.*, 315, 30-40.

Trauth, M. H., R. Gebbers, N. Marwan, and E. Sillmann (2007), MATLAB recipes for earth sciences, vol. 34, , Springer.

Walker, M., S. Johnsen, S. O. Rasmussen, T. Popp, J. Steffensen, P. Gibbard, W. Hoek, J. Lowe, J. Andrews, and S. Björck (2009), Formal definition and dating of the GSSP (Global Stratotype Section and Point) for the base of the Holocene using the Greenland NGRIP ice core, and selected auxiliary records, *Journal of Quaternary Science*, 24(1), 3-17.

WGMS (1988): Fluctuations of Glaciers 1980-1985 (Vol. V). Haeberli, W. and Müller, P. (eds.), IAHS (ICSI) / UNEP / UNESCO, World Glacier Monitoring Service, Zurich, Switzerland: 290 pp.

[\[pdf\]](#)

WGMS (1993): Fluctuations of Glaciers 1985-1990 (Vol. VI). Haeberli, W. and Hoelzle, M. (eds.), IAHS (ICSI) / UNEP / UNESCO, World Glacier Monitoring Service, Zurich, Switzerland: 322 pp.

[\[pdf\]](#)

WGMS (1998): Fluctuations of Glaciers 1990-1995 (Vol. VII). Haeberli, W., Hoelzle, M., Suter, S. and Frauenfelder, R. (eds.), IAHS (ICSI) / UNEP / UNESCO, World Glacier Monitoring Service, Zurich, Switzerland: 296 pp. [\[pdf\]](#)

WGMS (2005): Fluctuations of Glaciers 1995-2000 (Vol. VIII). Haeberli, W., Zemp, M., Frauenfelder, R., Hoelzle, M. and Kääb, A. (eds.), IUGG (CCS) / UNEP / UNESCO, World Glacier Monitoring Service, Zurich, Switzerland: 288 pp. [\[pdf\]](#)

WGMS (2008): Fluctuations of Glaciers 2000-2005 (Vol. IX). Haeberli, W., Zemp, M., Kääb, A., Paul, F. and Hoelzle, M. (eds.), ICSU (FAGS) / IUGG (IACS) / UNEP / UNESCO / WMO, World Glacier Monitoring Service, Zurich, Switzerland: 266 pp. [\[pdf\]](#)

WGMS (2012): Fluctuations of Glaciers 2005-2010 (Vol. X). Zemp, M., Frey, H., Gärtner-Roer, I., Nussbaumer, S.U., Hoelzle, M., Paul, F. and W. Haeberli (eds.), ICSU (WDS) / IUGG (IACS) / UNEP / UNESCO / WMO, World Glacier Monitoring Service, Zurich, Switzerland: 336 pp. Publication based on database version: doi:10.5904/wgms-fog-2012-11 [\[pdf\]](#)

Zemp, M., M. Hoelzle, and W. Haeberli (2007), Distributed modelling of the regional climatic equilibrium line altitude of glaciers in the European Alps, *Global Planet. Change*, 56(1), 83-100.